VACCINES

Dendritic cell–targeted lentiviral vector immunization uses pseudotransduction and DNA-mediated STING and cGAS activation

Jocelyn T. Kim,[1,2] Yarong Liu,[3] Rajan P. Kulkarni,[1,4] Kevin K. Lee,[1] Bingbing Dai,[3] Geoffrey Lovely,[1] Yong Ouyang,[1] Pin Wang,[3] Lili Yang,[1,5] David Baltimore[1]*

Dendritic cell (DC) activation and antigen presentation are critical for efficient priming of T cell responses. Here, we study how lentiviral vectors (LVs) deliver antigen and activate DCs to generate T cell immunization in vivo. We report that antigenic proteins delivered in vector particles via pseudotransduction were sufficient to stimulate an antigen-specific immune response. The delivery of the viral genome encoding the antigen increased the magnitude of this response in vivo but was irrelevant in vitro. Activation of DCs by LVs was independent of MyD88, TRIF, and MAVS, ruling out an involvement of Toll-like receptor or RIG-I–like receptor signaling. Cellular DNA packaged in LV preparations induced DC activation by the host STING (stimulator of interferon genes) and cGAS (cyclic guanosine monophosphate–adenosine monophosphate synthase) pathway. Envelope-mediated viral fusion also activated DCs in a phosphoinositide 3-kinase–dependent but STING-independent process. Pseudotransduction, transduction, viral fusion, and delivery of cellular DNA collaborate to make the DC-targeted LV preparation an effective immunogen.

INTRODUCTION

Dendritic cells (DCs) are targets for immunization purposes because of their superior ability to process antigens and present them to T cells. One strategy uses an HIV-1–derived lentiviral vector (LV) to deliver genes encoding antigen to DCs by pseudotyping the vector with a mutant DC-targeting Sindbis virus glycoprotein (SVGmu) (*1*, *2*). The in vivo administration of this LV resulted in the selective expression of antigen in DCs and efficient priming of antigen-specific $CD8^+$ T cells with antitumor immunity in mice in comparison with methods using recombinant protein antigen or adoptive transfer of antigen-loaded or viral vector–transduced DCs. DC-targeted LV vaccines are under clinical evaluation in humans (*3*). However, the exact mechanism behind such immunization is unclear. It is evident that antigen delivery methods lacking a DC maturation signal—such as antigen conjugated to the DC-specific anti–DEC-205 antibody—led to effective antigen presentation but promoted tolerance rather than immunity (*4*, *5*). The coadministration of a maturation stimulus was required to break immune tolerance (*4*). Thus, the efficacy of DC-targeted LV immunization likely requires the coupling of two independent functions: delivery of antigen and activation of DCs.

The first function—LV antigen delivery to DCs—is thought to primarily occur by transduction, which requires overcoming host restriction factors such as SAMHD-1 that block reverse transcription (*6*). Barriers to transduction are surmountable by using precursor DCs, high multiplicity of infection (MOI), or codelivering Vpx (*7*–*10*). Other mechanisms may enable delivery of protein antigens to DCs independent of transduction.

The second function—LV activation of DCs—can occur in well-differentiated DCs and with high MOI (*7*, *8*, *11*). LV nucleic acids can be detected by intracellular pathways involving endosomal Toll-like receptors (TLRs) (*12*–*14*), mitochondrial antiviral-signaling protein (MAVS) (*15*), cyclic guanosine monophosphate–adenosine monophosphate synthase (cGAS), and stimulator of interferon genes (STING) (*16*–*18*). However, lentivirus-like particles, which were deficient of viral nucleic acids, elicited potent antigen-specific $CD8^+$ T cells responses, suggesting that vector components other than viral nucleic acids contribute to DC activation (*19*–*21*).

In this study, we report that LV pseudotransduction was a key mechanism of antigen delivery and immune stimulation. LV transduction contributed to antigen delivery in vivo but was not required for immune stimulation. LVs induced DC activation via two processes. First, viral envelope–mediated fusion itself induced a phosphoinositide 3-kinase (PI3K)–dependent and STING-independent pathway. Second, we find that the human genomic DNA within virion preparations activated the STING and cGAS pathway.

RESULTS

LV pseudotransduction activates DCs

We first sought to understand the mechanism of antigen delivery to DCs generated at day 8 of culture with LV encoding green fluorescent protein (GFP) pseudotyped with vesicular stomatitis virus glycoprotein (VSV-G) or SVGmu (*1*). Culture of mouse bone marrow cells in granulocyte-macrophage colony-stimulating factor (GM-CSF) generated a heterogeneous population of which 70% were well-differentiated bone marrow–derived DCs (BMDCs) based on the expression of CD11c and CD11b (fig. S1A). Human monocytes cultured in GM-CSF and interleukin-4 (IL-4) generated a cell population composed of 96% monocyte-derived DCs (moDCs) based on negative expression of CD14 and positive expression of DC-SIGN (fig. S1B). Well-differentiated mouse BMDCs and human moDCs were difficult to transduce in vitro, but up to an eightfold increase in GFP mean fluorescence intensity (MFI) was observed [Fig. 1, A (top) and B

[1]Division of Biology and Biological Engineering, California Institute of Technology, Pasadena, CA 91125, USA. [2]Division of Infectious Diseases, Department of Medicine at University of California, Los Angeles, Los Angeles, CA 90095, USA. [3]Mork Family Department of Chemical Engineering and Materials Science, University of Southern California, Los Angeles, CA 90089, USA. [4]Division of Dermatology, Department of Medicine, David Geffen School of Medicine at University of California, Los Angeles, Los Angeles, CA 90095, USA. [5]Department of Microbiology, Immunology, and Molecular Genetics, University of California, Los Angeles, Los Angeles, CA 90095, USA.
*Corresponding author. Email: baltimo@caltech.edu

(left)] and undiminished by reverse transcriptase inhibitors (RTIs) [Fig. 1, C (top) and D]. By contrast, 293T cells treated with the same dose of LVs were efficiently transduced with up to a 21-fold increase in GFP MFI in a process that was sensitive to RTIs [Fig. 1, C (top right) and D (right)]. The GFP expression in BMDCs was dependent on the dose of LVs but not on whether the LVs were from unconcentrated or concentrated preparations (fig. S2A). In addition, GFP expression in BMDCs was highest immediately after LV treatment and

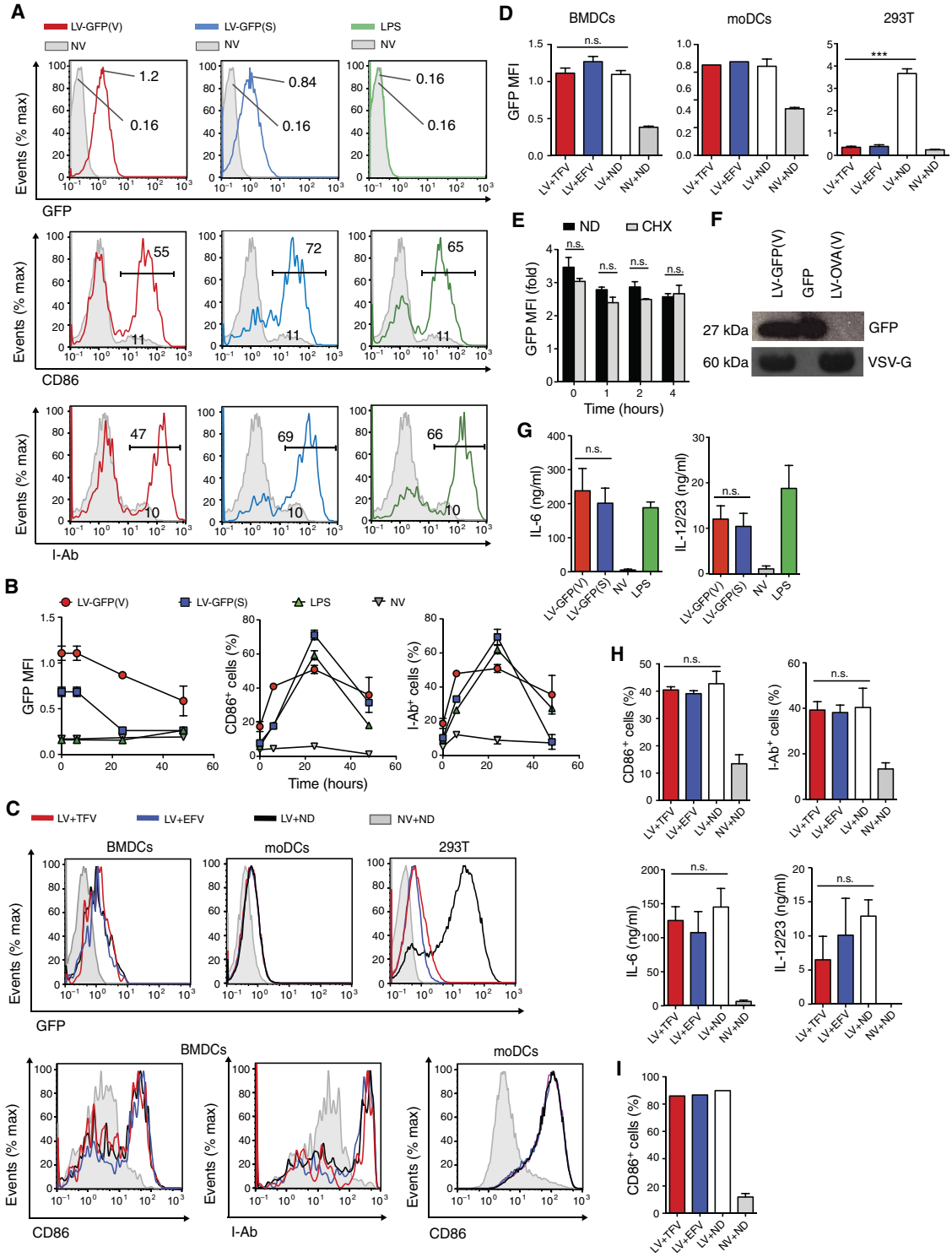

Fig. 1. LV pseudotransduction delivers proteins and activates DCs. (**A**) Representative fluorescence-activated cell sorting (FACS) plots of mouse BMDCs that were treated with LV-GFP(V), LV-GFP(S), LPS, or no vector (NV) and analyzed for expression of GFP, CD86, and I-Ab. GFP geometric MFI was measured immediately after LV spin inoculation, and CD86 and I-Ab expression was measured 24 hours after LV treatment. (**B**) GFP, CD86, and I-Ab expression of LV-treated BMDCs was measured over 48 hours. (**C**) Representative FACS plots of mouse BMDCs, human moDCs, and 293T cells that were incubated with tenofovir (TFV; 40 μM), efavirenz (EFV; 80 μM), or no drug (ND) 6 hours before treatment with LV-GFP(V) and then analyzed 24 hours later. (**D**) Graph depicts the GFP MFI of BMDCs, moDCs, and 293T cells from (C). (**E**) Mouse BMDCs were incubated with or without cycloheximide (CHX; 50 μg ml^{-1}) 1 hour before treatment with LV-GFP(V), and then, GFP MFI was presented relative to those BMDCs receiving no LV with or without cycloheximide. (**F**) Western blot analysis of GFP of lysates from LV-GFP(V) and LV expressing OVA pseudotyped with VSV-G [LV-OVA(V)] and purified GFP protein (40 ng). (**G**) Mouse BMDCs were treated as in (A) and analyzed for the amount of IL-6 and IL-12/23 in the supernatant by ELISA 24 hours after LV treatment. (**H** and **I**) Mouse BMDCs (H) and human moDCs (I) were treated as in (C) and analyzed for expression of CD86, I-Ab, or amount of IL-12/23 and/or IL-6 in the supernatant 24 hours after LV treatment. Data are representative of two (A to D and G to I) or three (E and F) independent experiments. Results are shown as mean ± SEM (B, D, E, G, and H). n.s., not significant. $P > 0.05$; $^{***}P < 0.001$ [one-way ANOVA (D and H) and unpaired Student's *t* test (E and G)].

then steadily decreased over 48 hours (Fig. 1B, left). Although LVs can deliver host cellular mRNA (*22*), we found that the protein synthesis inhibitor cycloheximide failed to decrease BMDC expression of GFP (Fig. 1E), suggesting that the GFP was not produced de novo in DCs. We could detect GFP in lysates of LV particles by Western blot analysis (Fig. 1F), finding about 1.53 μg of GFP per microgram of p24 by enzyme-linked immunosorbent assay (ELISA). These results are consistent with previous reports that LVs were capable of pseudotransduction (*23*, *24*).

We next sought to determine whether LV pseudotransduction was important to DC activation. Consistent with previous work, we found that mouse BMDCs were activated by LVs, as demonstrated by the increase expression of activation markers CD86 and major histocompatibility complex II (MHC II) molecule and secretion of cytokines IL-6 and IL-12/23 [Fig. 1, A (middle and bottom), B (middle and right), and G] (*1*, *14*) in a dose-dependent manner (fig. S2B). DC activation was similar between unconcentrated and concentrated LV preparations (fig. S2B). Pseudotransduction occurred in both well- and less-differentiated BMDCs (fig. S3A), but LV activation occurred only among the well-differentiated DCs (fig. S3B). LV activation of mouse BMDCs and human moDCs was not diminished by RTIs [Fig. 1, C (bottom), H, and I], suggesting that LVs activated DCs via a reverse transcriptase–independent mechanism. This lack of sensitivity to RTIs was not due to ineffective inhibition

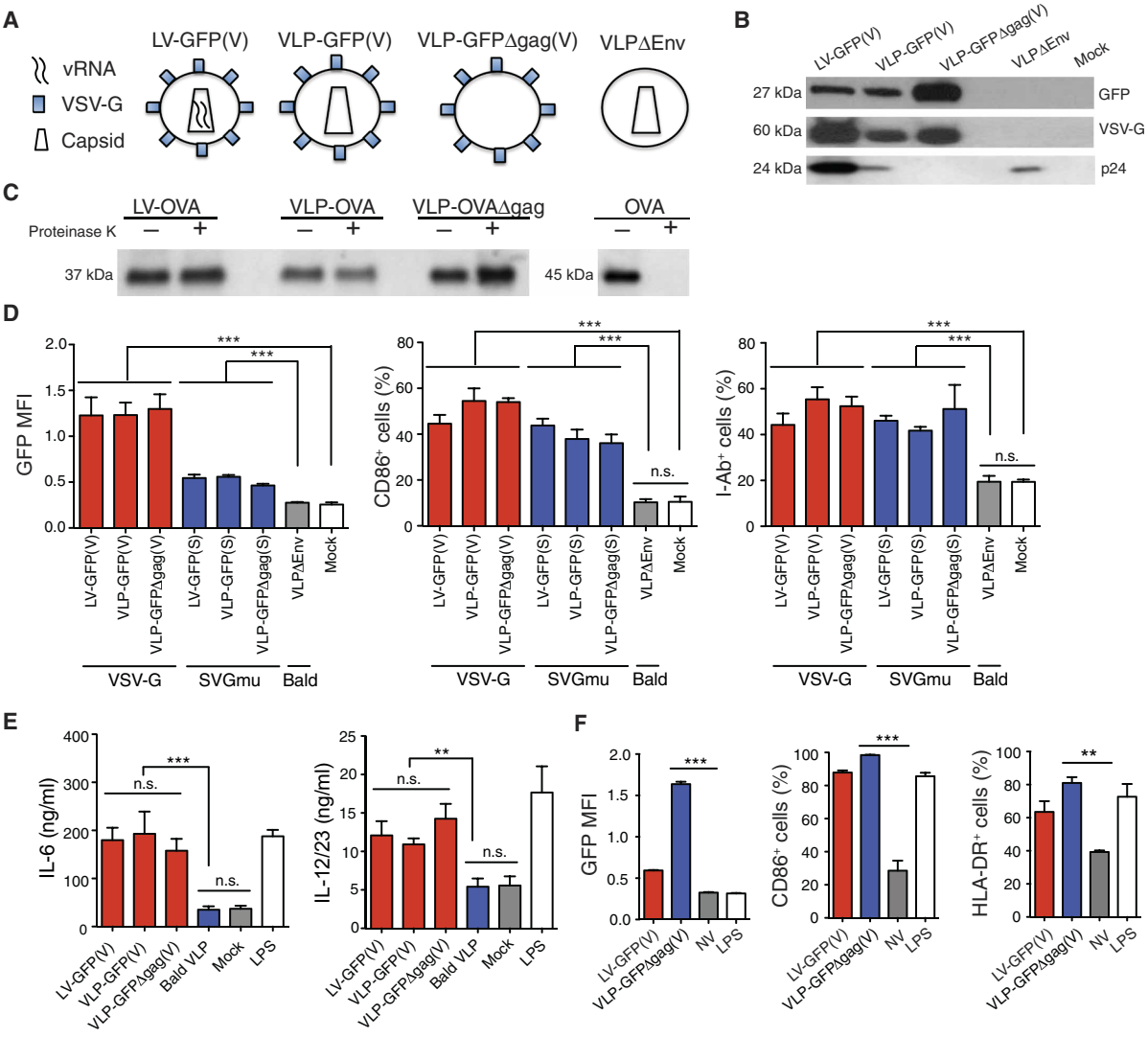

Fig. 2. LV envelope is responsible for DC activation. (**A**) Schematic of components of LV and VLPs. (**B**) Western blot analysis for GFP, VSV-G, and p24 on LV and VLP lysates. (**C**) Western blot analysis detecting OVA in the lysate of the following SVGmu-pseudotyped vectors: LV carrying OVA (LV-OVA), VLP carrying OVA (VLP-OVA), and VLP-carrying OVA deficient of gag (VLP-OVAΔgag). Vectors were treated or not treated with proteinase K, which was inactivated with PMSF before vector lysis. To verify whether proteinase K degradation was effective, we used soluble OVA as a control. (**D** and **E**) Mouse BMDCs were treated with VSV-G or SVGmu-pseudotyped LVs and VLPs and then analyzed at 24 hours for GFP, CD86, and I-Ab expression by flow cytometry (D) and for the amount of IL-6 and IL-12/23 in the cell supernatant by ELISA (E). (**F**) Human moDCs were treated with LV-GFP(V) or VLP carrying GFP deficient of gag [VLP-GFPΔgag(V)] and analyzed at 24 hours for GFP, CD86, and human MHC II molecule human lymphocyte antigen-D–related (HLA-DR) expression by flow cytometry. Data are representative of three (B and C) or two (D to F) independent experiments. Results are shown as mean ± SEM. $P > 0.05$; $^{**}P < 0.005$; $^{***}P < 0.001$ (unpaired Student's *t* test).

of reverse transcription because the RTIs blocked GFP transduction in LV-infected 293T cells [Fig. 1, C (top right) and D (right)].

To determine the LV component responsible for DC activation, we generated a platform of genome-less virus-like particles (VLPs) by omitting plasmids encoding the viral genome, capsid, or envelope (Fig. 2A) (*13*, *25*). We confirmed the presence of the viral envelope and capsid by detecting VSV-G and p24, respectively, using Western blot analysis (Fig. 2B). Similar to LVs, we found that pseudotyped VLPs incorporated the vector-encoded proteins GFP or ovalbumin (OVA) but not "bald" viral particles that were produced by transfecting 293T cells with only the packaging plasmids encoding gag, pol, and rev. To assess whether these proteins were carried within the vectors or associated externally, we treated LV and VLPs incorporating OVA with proteinase K, inactivated the proteinase K with phenylmethylsulfonyl fluoride (PMSF), lysed the vectors, and still detected OVA in the lysate, indicating that the OVA in vectors was proteinase K–resistant and thus carried within particles (Fig. 2C). An OVA suspension, which was not associated with vectors, was not proteinase K–resistant. We next found that the pseudotyped VLPs but not "bald" VLPs delivered GFP and induced the activation of mouse BMDCs (Fig. 2, D and E). The inclusion of the vector genome or viral capsid into the VLP had no effect on BMDC activation [Fig. 2, D (middle and right) and E]. Furthermore, VSV-G–pseudotyped VLPs capably delivered GFP and activated human moDCs (Fig. 2F). Together, these data suggest that the viral envelope, but not the vector genome or capsid, was necessary and sufficient to activate DCs.

LV genome, cDNA, and capsid are not adjuvants in vivo

To determine whether these findings were relevant in vivo, we injected into mice the DC-targeted SVGmu-pseudotyped LV-OVA with or without a concurrent oral regimen of RTIs or VLP carrying OVA pseudotyped with SVGmu (VLP-OVA). We initially found that OVA-specific $CD8^+$ T cells were similarly induced in all three groups at 7 days after immunization (Fig. 3A and fig. S1C). However, through 10 days after immunization, the magnitude of these cells continued to increase in LV-immunized mice but not in mice immunized with LV-OVA with RTIs or VLP (Fig. 3A), suggesting that transduction was enhanced, but was not necessary, for inducing antigen-specific $CD8^+$ T cells. After the second administration of homologous vector, the OVA-specific $CD8^+$ T cells were boosted in all three groups (Fig. 3A, right) and expressed similar effector memory phenotypes ($CD62L^{lo}CD44^{hi}$) (Fig. 3B). After the secondary immune responses subsided, we injected 5×10^6 OVA-expressing E.G7 thymoma tumor cells and 5×10^6 control non–OVA-expressing EL4 thymoma tumor cells on opposing legs, enabling intra-animal comparison. Mice homologously prime-boosted with LV with or without RTIs or VLPs were protected against the growth of OVA-expressing E.G7 tumors (Fig. 3C, left). As expected, non–OVA-expressing EL4 tumors continued to grow in the immunized mice (Fig. 3C, right). The antitumor protection of mice immunized with LV with RTI and VLP was not altogether unexpected because 8 to 10% of the $CD8^+$ T cells were OVA-specific after the boost. The similar immunization responses of mice receiving LV with RTIs and VLP demonstrate that a component of LV immunization was independent of reverse transcription and the viral genome, likely due to pseudotransduction. We next found that immunization responses were similar between mice homologously prime-boosted with VLPs carrying OVA with or without the viral capsid (VLP-OVA or VLP-OVAΔgag, respectively) (Fig. 3, D and E). Therefore, VLPs, which had the viral envelope as the sole viral component, generated a strong-enough memory $CD8^+$ T cell response to be protective against the growth of OVA-expressing E.G7 tumor cells (Fig. 3F). The viral capsid did not enhance immunization responses.

We next questioned why LV-immunized mice had a greater immune response compared with mice treated with LV with RTI or VLP. We generated an SVGmu-pseudotyped LV encoding GFP and carrying the protein OVA (LV-GFP^{gene}-$OVA^{protein}$). Because the vector-generated LV DNA did not encode OVA, we could assess whether LV DNA enhances OVA pseudotransduction. This vector induced an OVA-specific $CD8^+$ T cell response similar to VLP-immunized mice but not LV-immunized mice, suggesting that reverse-transcribed LV DNA did not enhance the antigen-specific $CD8^+$ T cell response produced by pseudotransduction (Fig. 3G). Together, these results suggest that LV genome transduction amplified antigen delivery but not immune stimulation in vivo.

The direct injection of SVGmu-pseudotyped LV into mice specifically transduces conventional DCs (cDCs) in vivo and not other immune cells (*1*, *26*, *27*). To assess whether DCs were pseudotransduced in vivo, we subcutaneously injected SVGmu-pseudotyped VLP carrying GFP into the hindleg of wild-type mice and, after 1 day, harvested lymphoid tissue to analyze cells for GFP expression. GFP-positive cells were detected in cDCs, particularly in the $CD11b^-$ and $CD11b^+$ cDC subsets, from the draining inguinal lymph nodes of VLP-immunized mice but not of unimmunized mice (figs. S1D and S4A). There was no obvious difference in GFP expression among the plasmacytoid DCs, B cells, T cells, or macrophages isolated from the lymph nodes of VLP-immunized and unimmunized mice (fig. S4). These results suggest that the DC-targeted vectors pseudotransduced cDCs in vivo.

LVs and VLPs activate DCs and adaptive immunity via the STING and cGAS pathway

We next set out to identify the innate immune signaling pathway responsible for LV detection. LVs capably activated BMDCs from mice deficient in MyD88, TRIF, or MAVS (Fig. 4A). Activation of BMDCs from mice doubly deficient in MyD88 and TRIF or MyD88 and MAVS was still unaffected (Fig. 4B). LV-OVA immunization of MyD88-, TRIF-, or MAVS-deficient mice capably induced OVA-specific effector memory $CD8^+$ T cells (Fig. 4, C and D). LV-OVA immunization of TLR4-deficient mice was also efficient (fig. S5, A to C). In addition, LVs capably activated BMDCs from mice lacking the interferon-α/β (IFN-α/β) receptor function (fig. S5D), indicating that type I IFN signaling was not required. We then turned to the STING and cGAS pathway and found that LV immunization was significantly decreased up to threefold in these mutant mice (Fig. 4, E and F), suggesting that STING and cGAS were important to LV immunization.

In addition, we observed that VLP activation of BMDCs was partially dependent on STING and cGAS (Fig. 5, A and B). STING- or cGAS-deficient BMDCs treated with VLP carrying OVA had a reduced ability to up-regulate the activation marker CD69 on $CD8^+$ T cells expressing an OVA-specific T cell receptor (Fig. 5, C and D, and fig. S1E). The homologous prime-boost vaccination of STING- or cGAS-deficient mice with the DC-targeted VLP-OVA induced up to threefold less effector memory $CD8^+$ T cells (Fig. 5, E to H). Mice deficient in MyD88 (*28*), TRIF (*29*), MAVS (*30*), type I IFN receptor (*31*), STING (*32*), or cGAS (*33*) are born at expected Mendelian ratios and grow without obvious developmental or fertility issues. BMDC populations generated in vitro among these mutants were represented similarly compared with wild-type BMDCs (fig. S6). Together, these results suggest that

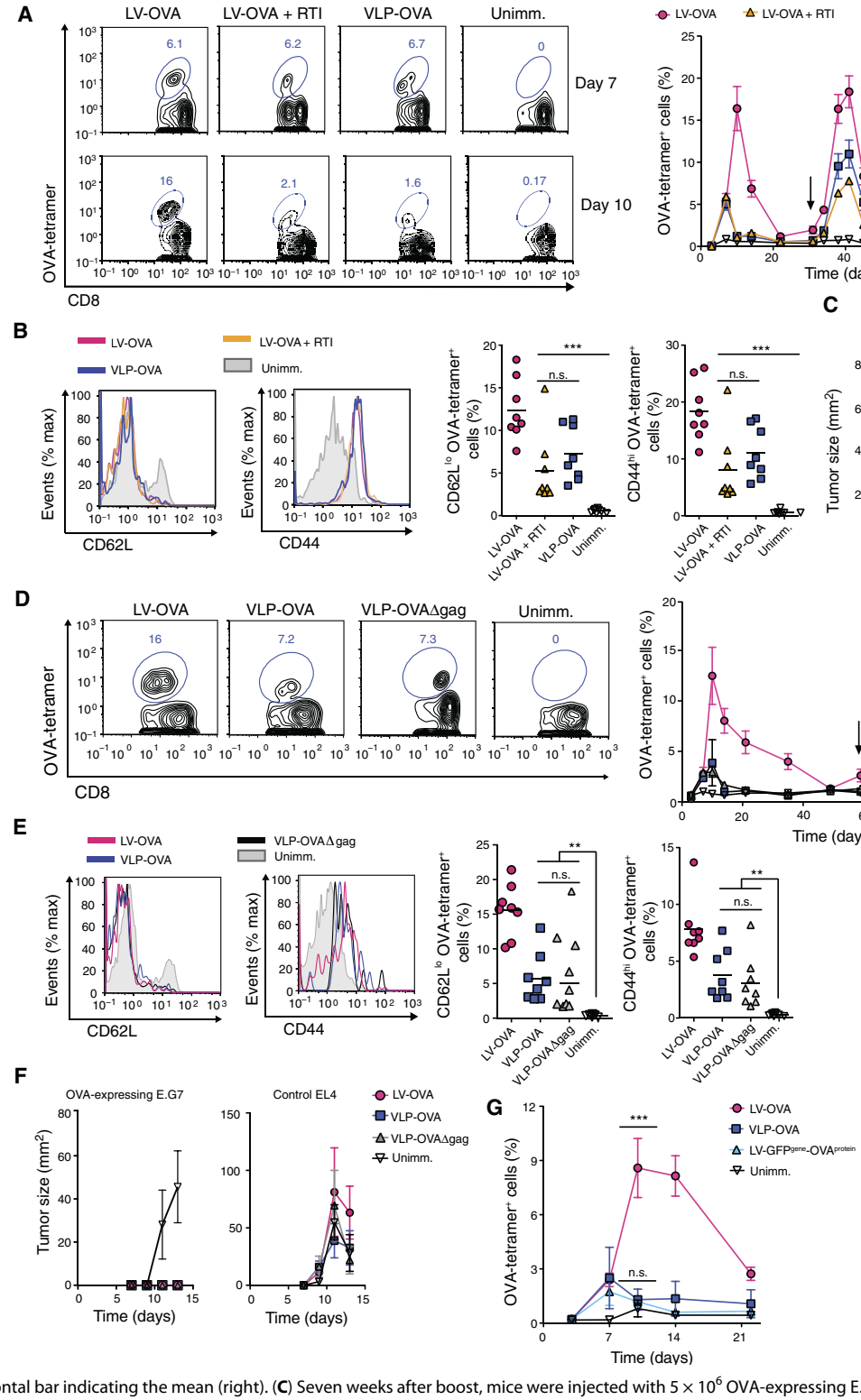

Fig. 3. LV DNA, genome, and capsid are not required for DC activation and CD8$^+$ T cell priming in vivo. (**A**) Wild-type mice received homologous prime-boost vaccination of SVGmu-pseudotyped LV-OVA with or without RTI or VLP-OVA ($n = 8$ mice per group). Representative FACS plots show OVA-tetramer$^+$ cells gated on CD8$^+$ T cells from the blood at 7 and 10 days after primary immunization (left). Graph depicts percentages of OVA-tetramer$^+$ CD8$^+$ T cells from the blood of immunized and unimmunized mice over time (black arrow, boost) (right). (**B**) Representative FACS plots show expression of CD62L and CD44 on OVA-tetramer$^+$ CD8$^+$ T cells from immunized mice compared with naïve CD8$^+$ T cells from unimmunized mice at 7 days after boost (left). Graphs depict percentages of CD62L^{lo} and CD44^{hi} OVA-tetramer$^+$ cells, with each symbol representing an individual mouse and horizontal bar indicating the mean (right). (**C**) Seven weeks after boost, mice were injected with 5×10^6 OVA-expressing E.G7 thymoma tumor cells and 5×10^6 EL4 (control) non–OVA-expressing EL4 thymoma tumor cells on opposing legs, and tumor sizes were measured. (**D** to **F**) Wild-type mice were homologously prime-boosted with LV-OVA, VLP-OVA, or capsid-less VLP-OVAΔgag. OVA-tetramer$^+$ cells from the blood were analyzed as in (A) ($n = 8$ mice per group) at 7 days after boost (left) and over time (right) (D). CD62L and CD44 expression of OVA-tetramer$^+$ CD8$^+$ T cells from immunized mice compared with naïve CD8$^+$ T cells from unimmunized mice at 7 days after boost were measured as in (B) (E). Mice were injected with tumor cells, as in (C), and tumor sizes were measured (F). (**G**) Wild-type mice were immunized with LV-OVA, LV encoding OVA carrying GFP (LV-GFP^{gene}-OVA^{protein}), or VLP-OVA ($n = 8$ mice per group), and OVA-tetramer$^+$ CD8$^+$ T cells from the blood were measured over time. Statistical comparisons were made between the LV-GFP^{gene}-OVA^{protein}– and VLP-OVA– or LV-OVA–immunized mice. Data are representative of two independent experiments (A to G). Results are shown as mean ± SEM (A, C, D, F, and G). $P > 0.05$; $^{**}P < 0.005$; $^{***}P < 0.001$ (unpaired Student's t test).

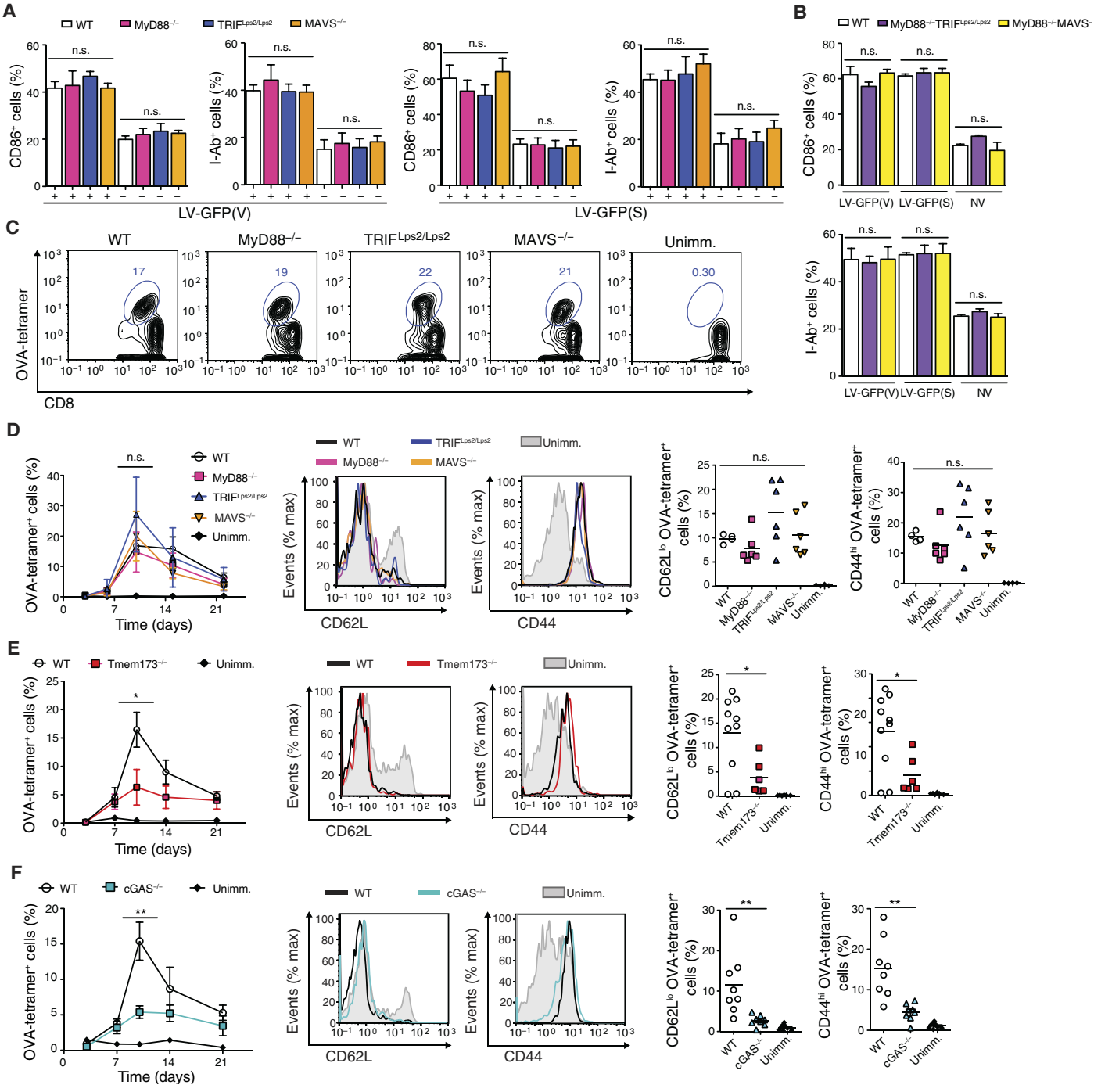

Fig. 4. LV activation of DCs and subsequent CD8$^+$ T cell priming are dependent on STING and cGAS but not on MyD88, TRIF, or MAVS. (**A** and **B**) BMDCs from mice singly or doubly deficient in MyD88, TRIF, and MAVS were treated with LV-GFP(V) or LV-GFP(S) and analyzed at 24 hours for expression of CD86 and I-Ab by flow cytometry. (**C** to **F**) Mice deficient in MyD88, TRIF, MAVS, STING, or cGAS were immunized with LV-OVA. Unimmunized wild-type (WT) mice were injected with PBS. OVA-tetramer$^+$ cells gated on CD8$^+$ T cells from the blood were demonstrated on representative FACS plot at 10 days after primary immunization (C) or measured over time (D to F) (left). Statistical comparisons were made between the OVA-tetramer$^+$ CD8$^+$ T cell response of the LV-immunized wild-type mice and that of the LV-immunized mutant mice. CD62L^{lo} and CD44^{hi} OVA-tetramer$^+$ CD8$^+$ T cells from LV-immunized mutant and wild-type mice were compared with naïve CD8$^+$ T cells from unimmunized mice at 10 days on representative FACS plots (D to F) (middle) or by group with each symbol representing an individual mouse and horizontal bar indicating the mean (D to F) (right). $n = 6$ mutant immunized mice per group; $n = 4$ wild-type immunized and unimmunized mice per group (C and D). $n = 6$ mice in Tmem173$^{-/-}$ immunized and unimmunized wild-type groups; $n = 10$ mice in wild-type immunized group (E). $n = 8$ per group (F). Data are representative of three (A and B) or two (C to E) independent experiments or pooled from two independent experiments (F). Results are shown as mean ± SEM (A, B, and D to F). $P > 0.05$; *$P < 0.05$; **$P < 0.005$ [one way-ANOVA (A, B, and D) and unpaired Student's t test (E and F)].

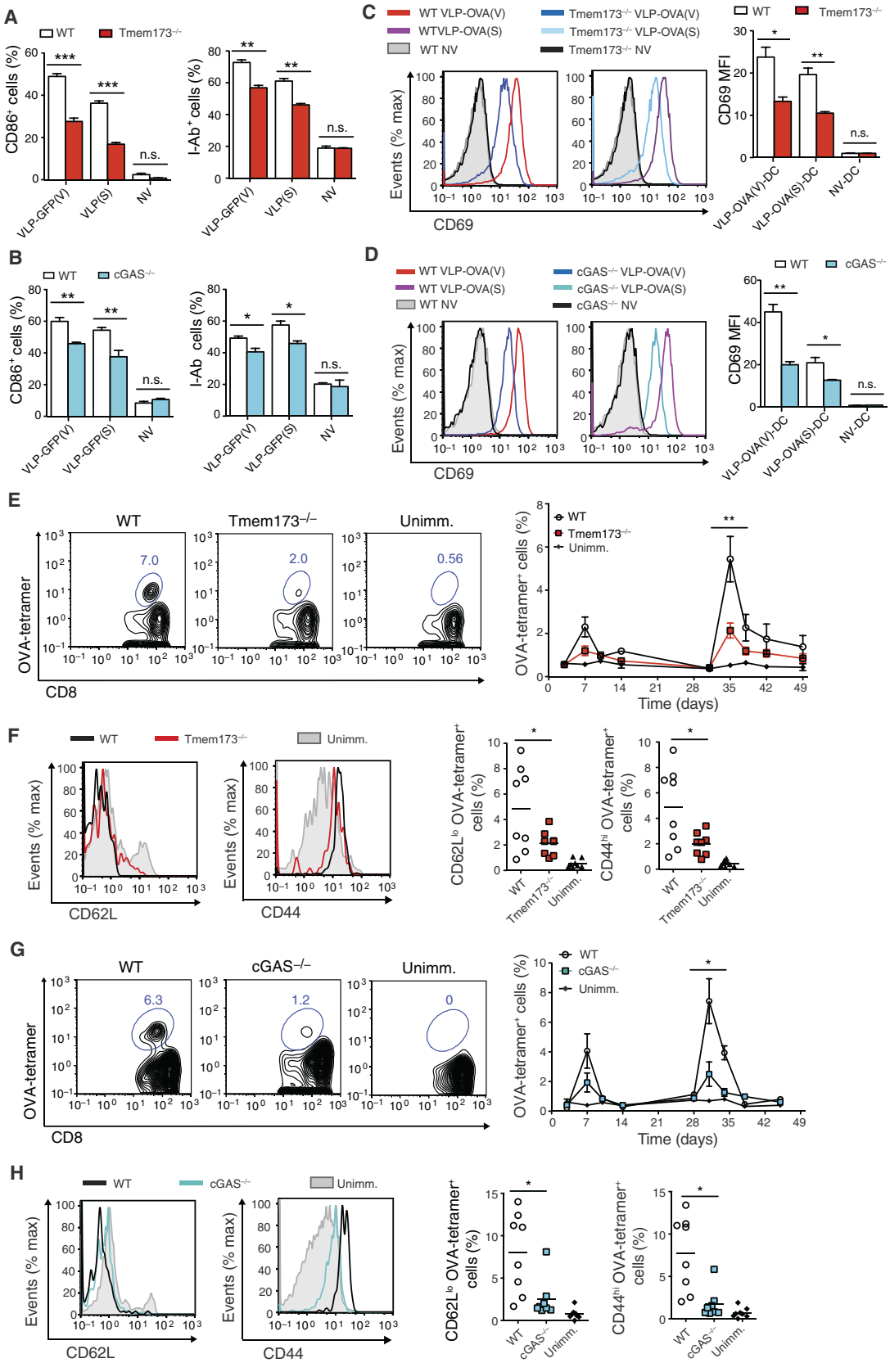

Fig. 5. VLPs activate DCs and antigen-specific CD8$^+$ T cells via the STING and cGAS pathway. (**A** and **B**) BMDCs from Tmem173$^{-/-}$ and cGAS$^{-/-}$ mice were treated with VLP-GFP(V) or VLP-GFP(S) and analyzed at 24 hours for CD86 and I-Ab expression by flow cytometry. (**C** and **D**) Tmem173$^{-/-}$ and cGAS$^{-/-}$ BMDCs were treated with VLP-OVA pseudotyped with VSV-G [VLP-OVA(V)] or SVGmu [VLP-OVA(S)] and then cocultured with OT-1 CD8$^+$ T cells for 24 hours. Representative FACS plots show expression of the T cell activation marker CD69 among the OT-1 CD8$^+$ T cells (C and D) (left). Graph depicts CD69 MFI of the OT-1 CD8$^+$ T cells (C and D) (right). (**E** to **H**) Tmem173$^{-/-}$, cGAS$^{-/-}$, and wild-type mice were homologously prime-boosted with SVGmu-pseudotyped VLP-OVA ($n = 8$ per group). OVA-tetramer$^+$ cells gated on CD8$^+$ T cells from the blood were demonstrated on representative FACS plot at 10 days after primary immunization (E and G) (left) or measured over time (E and G) (right) (black arrow, boost). Statistical comparisons were made between the OVA-tetramer$^+$ CD8$^+$ T cell response of the VLP-immunized wild-type and VLP-immunized mutant mice. CD62L^{lo} and CD44^{hi} OVA-tetramer$^+$ CD8$^+$ T cells from LV-immunized Tmem173$^{-/-}$, cGAS$^{-/-}$, and wild-type mice were compared with naïve CD8$^+$ T cells from unimmunized wild-type mice at 10 days on representative FACS plots (F and H) (left) or by group with each symbol representing an individual mouse and horizontal bar indicating the mean (F and H) (right). Data are representative of two independent experiments (A to H). Results are shown as mean ± SEM (A to E and G). $P > 0.05$; *$P < 0.05$; **$P < 0.005$; ***$P < 0.001$ (unpaired Student's t test).

a component within LVs, which is not the viral genome, triggered the host STING and cGAS pathway.

Viral fusion is required for DC activation

VSV and Sindbis virus release viral contents into the cytosol through pH-dependent fusion between the viral envelope and the host endosomal membrane (*34*, *35*). LV and VLP activation of BMDCs was abolished in the presence of chloroquine, an inhibitor of endosomal acidification and viral fusion (Fig. 6A). This effect was not due to lack of vector internalization into endosomes because intracellular punctate GFP was evident in LV- and VLP-treated cells receiving chloroquine by microscopy (Fig. 6B). We also generated vectors pseudotyped with an altered VSV-G, in which mutations rendered the envelope fusion-defective without affecting envelope binding or receptor-mediated endocytosis (*36*). BMDCs treated with fusion-defective VLP showed punctate GFP presence similar to VLP- and chloroquine-treated cells, whereas BMDCs treated with fusion-competent VLP displayed diffuse intracellular GFP presence (Fig. 6B). The fusion-defective LV and VLP failed to activate mouse BMDCs (Fig. 6C), suggesting that viral fusion was required for the activation of DCs.

We next asked whether the viral process of membrane fusion itself and/or the release of a putative activating component into the cytosol represented the activating stimuli. We incorporated VSV-G into the lipid membrane of noncationic multilamellar liposomes, which allowed for the liposomal contents to evade lysosomal degradation and be delivered into the cytosol via viral envelope–directed fusion (*37*). The delivery of GFP and activation of mouse BMDCs were greatly enhanced if the liposomes were enveloped with VSV-G (Fig. 6D), indicating that VSV-G–directed fusion itself was immunostimulatory. DC activation was unaffected in STING-deficient mouse BMDCs treated with VSV-G liposomes (Fig. 6E), which suggests that VSV-G–directed fusion induced DC activation independent of STING.

We next examined the role of PI3K in VSV-G fusion–induced DC activation given its role in viral fusion and DC activation (*38*). We found that DC activation by VSV-G–pseudotyped VLP was, in part, inhibited by the PI3K inhibitor, LY292004 (Fig. 6F). In addition, we observed that VSV-G–pseudotyped VLPs were capable of inducing phosphorylation of PI3K but not fusion-defective VLPs (fig. S7A). VSV-G–pseudotyped LVs capably transduced 293T cells treated in the presence of LY292004 (fig. S7B), which is consistent with previous work demonstrating that the entry and fusion of VSV-G–pseudotyped vectors are PI3K-independent (*39*, *40*). Thus, these results suggest that activation of PI3K occurred downstream of viral fusion. To assess whether STING or cGAS was involved in this fusion-induced PI3K-dependent pathway, we treated BMDCs from mice deficient in STING or cGAS with VSV-G–pseudotyped VLPs in the presence of LY292004. Activation was partially decreased in the VLP-treated STING-deficient BMDCs and then further decreased with the addition of LY292004 (Fig. 6G), suggesting that the VSV-G fusion and PI3K-dependent pathway were largely independent of STING and cGAS. Together, these data suggest that there are two pathways contributing to VLP activation of DCs: one that is fusion- and PI3K-dependent and one that is STING- and cGAS-dependent.

Human genomic DNA carried by lentiviral particles and VLPs is immunostimulatory

We next sought to identify the stimulatory viral component that was released into the cytoplasm by viral fusion and was responsible for activating STING and cGAS. We amplified plasmid-specific and human genomic DNA sequences from the vector preparations (Fig. 7A) (*13*). We did not find evidence of human DNA in cell-free supernatant collected from 293T cells transfected with a mock plasmid. To assess whether the DNA was carried within or associated externally to the particles, we pretreated VLPs with deoxyribonuclease I (DNase I) to degrade external DNA and then inactivated DNase I with EDTA before the particles were lysed and then analyzed by polymerase chain reaction (PCR). Despite pretreatment with DNase I, we continued to detect plasmid and human DNA in the vector preparations, suggesting that this DNA was contained within the particles (Fig. 7B). We used genomic DNA to show that DNase I digestion and EDTA inactivation were effective (Fig. 7C). In addition, we detected about 150 ng of double-stranded DNA (dsDNA) per microliter and 12 ng of single-stranded DNA per microliter of the concentrated LV preparation (fig. S8A). The DNA extracted from the vector preparation appeared to be mostly composed of fragments of less than 10 kb, whereas genomic DNA extracted from cells was of longer fragments greater than 10 kb (fig. S8B). Deep sequencing of the DNA extracted from the viral particles demonstrated that about 99% of the reads were mapped to the human genome, whereas about only 1% of the reads were mapped to plasmid DNA (fig. S8C). Of the reads that were mapped to the human genome, there appeared to be a random distribution across the human chromosomes (fig. S8D). These results suggest that the DNA within LV preparations was predominantly double-stranded, fragmented, human genomic in origin, and incorporated into the viral particles randomly.

We also amplified plasmid and human DNA in HIV-1 produced from 293T cell transfection (Fig. 7D). To determine whether the presence of genomic DNA in vector particles was particular to the transfection process, we passaged HIV-1 in human peripheral blood mononuclear cells (PBMCs) and amplified human DNA from the cell-free HIV-1 supernatant (Fig. 7E). Human DNA was not detected in the cell-free supernatant collected from uninfected PBMCs. In addition, some of the DNA detected in the passaged cell-free HIV-1 supernatant was resistant to DNase I (Fig. 7F), suggesting that human genomic DNA was also encapsulated inside HIV-1 particles.

We next questioned whether the delivery of plasmid or genomic DNA by viral fusion would enhance the DC activation generated by viral fusion itself. We treated mouse BMDCs with empty VSV-G liposomes or VSV-G liposomes carrying intact plasmid DNA or genomic DNA extracted from 293T cells. Human genomic DNA enhanced the immunogenicity of the fusogenic liposomes in wild-type BMDCs (Fig. 7G), which was abrogated in STING-deficient BMDCs (Fig. 7H). The addition of intact plasmid DNA to fusogenic liposomes did not enhance BMDC activation (Fig. 7G). Furthermore, LVs generated by either transient transfection using plasmids or plasmid-free packaging system similarly stimulated wild-type BMDCs (Fig. 7I), suggesting that plasmid DNA within the vector preparations was not likely a dominant activator of DCs. LVs generated by plasmid DNA–free cell lines capably stimulate innate and adaptive immune responses in vivo (*41*, *42*). These findings provide an explanation for the STING and cGAS dependence observed in the innate and adaptive immune responses generated by LVs and VLPs.

DISCUSSION

In the present investigation, we found that vector-encoded protein antigen carried by vector particles via pseudotransduction sufficiently delivered antigen and stimulated the immune system. LV transduction

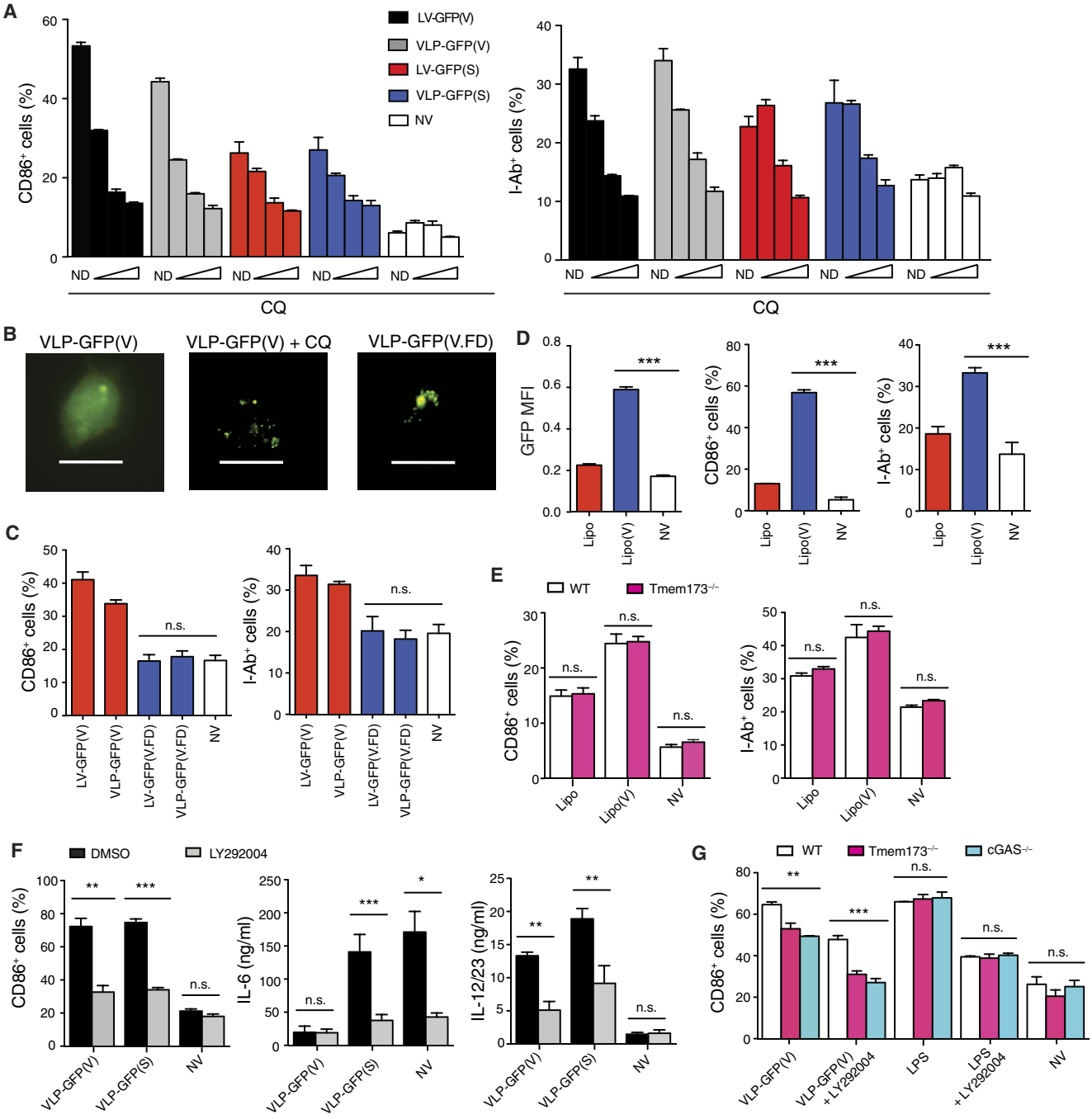

Fig. 6. Viral fusion is required for DC activation. (**A**) BMDCs from wild-type mice were incubated with chloroquine (CQ) at 25, 75, 100 μM (wedges) or with no drug 1 hour before treatment with LV or VLPs and analyzed at 24 hours for CD86 and I-Ab expression by flow cytometry. (**B**) Fluorescence microscopy was used to analyze GFP expression in wild-type mouse BMDCs treated with fusion-competent VLP-GFP(V) with or without chloroquine (100 μM) or the fusion-defective VLP, VLP-GFP(V.FD). Magnification, ×400. Scale bars, 10 μm. (**C**) Wild-type mouse BMDCs were treated with fusion-competent or fusion-defective LVs or VLPs carrying GFP and analyzed for CD86 and I-Ab expression by flow cytometry. (**D** and **E**) BMDCs from wild-type and Tmem173$^{-/-}$ mice were treated with naked (Lipo) or VSV-G–enveloped multilamellar liposomes [Lipo(V)] carrying GFP and analyzed at 24 hours for CD86 and I-Ab expression by flow cytometry. (**F**) Wild-type mouse BMDCs were treated with VSV-G– or SVGmu-pseudotyped VLPs with or without LY292004 (50 μM) and analyzed for CD86 expression by flow cytometry and for the amount of IL-12/23 and IL-6 in the supernatant by ELISA. (**G**) BMDCs from Tmem173$^{-/-}$, cGAS$^{-/-}$, and wild-type mice were treated with VSV-G–pseudotyped VLP or LPS (100 ng ml^{-1}) with or without LY292004 (50 μM) and analyzed for CD86 expression by flow cytometry. Data are representative of three independent experiments (A to D) or two independent experiments (E to G). Results are shown as mean ± SEM (A and C to G). $P > 0.05$; *$P < 0.05$; **$P < 0.005$; ***$P < 0.001$ [one way-ANOVA (C and G) and unpaired Student's t test (D to F)].

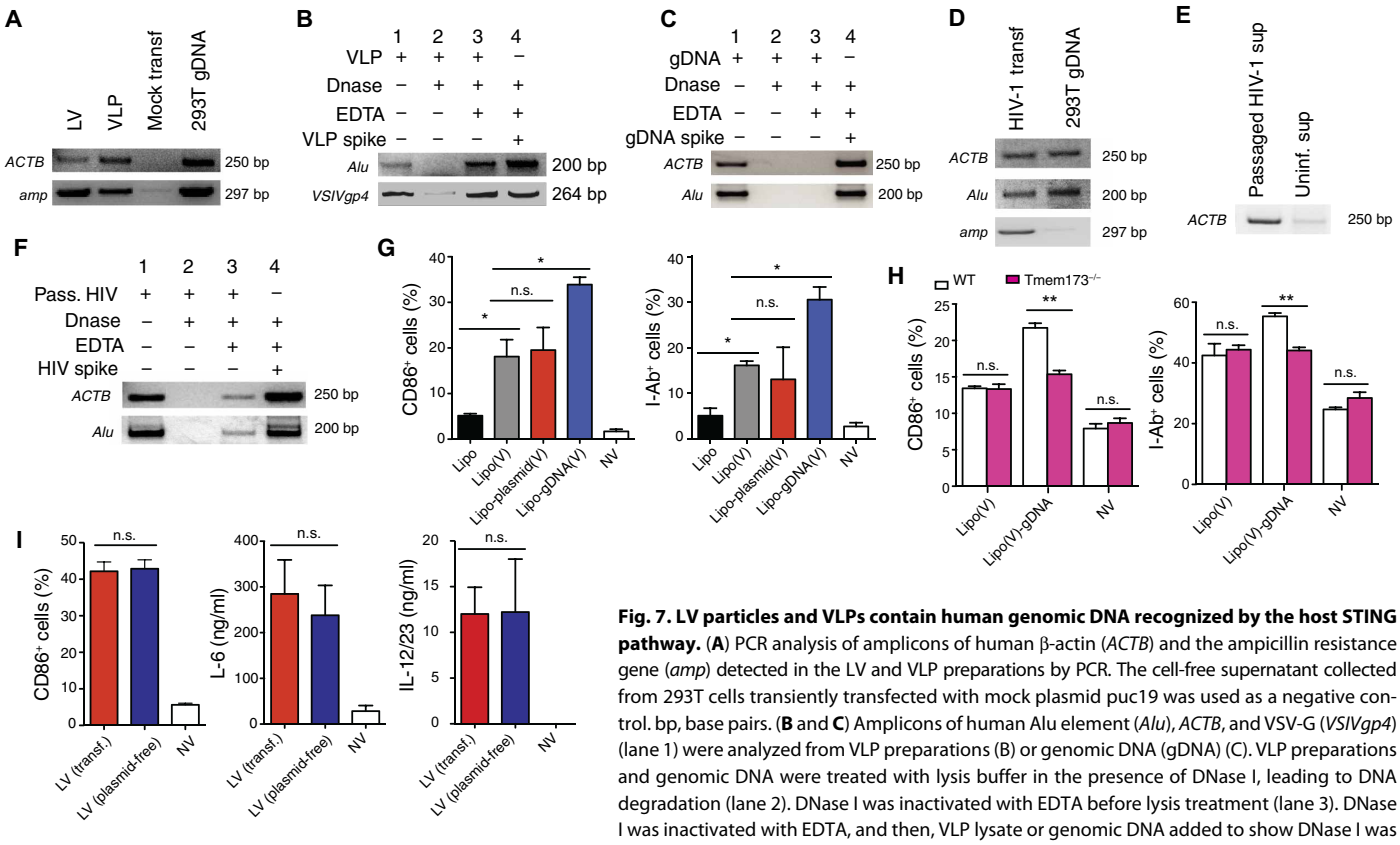

Fig. 7. LV particles and VLPs contain human genomic DNA recognized by the host STING pathway. (**A**) PCR analysis of amplicons of human β-actin (*ACTB*) and the ampicillin resistance gene (*amp*) detected in the LV and VLP preparations by PCR. The cell-free supernatant collected from 293T cells transiently transfected with mock plasmid puc19 was used as a negative control. bp, base pairs. (**B** and **C**) Amplicons of human Alu element (*Alu*), *ACTB*, and VSV-G (*VSIVgp4*) (lane 1) were analyzed from VLP preparations (B) or genomic DNA (gDNA) (C). VLP preparations and genomic DNA were treated with lysis buffer in the presence of DNase I, leading to DNA degradation (lane 2). DNase I was inactivated with EDTA before lysis treatment (lane 3). DNase I was inactivated with EDTA, and then, VLP lysate or genomic DNA added to show DNase I was effectively inactivated (lane 4). (**D**) Amplicons of *ACTB*, *Alu*, and *amp* were analyzed on HIV-1 supernatant collected from 293T cells transiently transfected with the plasmid encoding infectious HIV-1 or 293T genomic DNA. (**E**) HIV-1 was passaged in primary PBMCs, and the cell-free supernatant was collected and analyzed for human *ACTB* by PCR. As a negative control, cell-free supernatant was collected from uninfected PBMCs. (**F**) Supernatant primary PBMCs passaged with HIV-1 were treated as in (B) and (C). (**G** and **H**) BMDCs from wild-type mice were treated with naked (Lipo) or VSV-G–enveloped multilamellar liposomes carrying plasmid DNA [Lipo-plasmid(V)], genomic DNA extracted from 293T cells [Lipo-gDNA(V)], or nothing [Lipo(V)] (G). BMDCs from Tmem173$^{-/-}$ or wild-type mice were treated with naked (Lipo) or VSV-G–enveloped multilamellar liposomes carrying plasmid DNA [Lipo-plasmid(V)], genomic DNA extracted from 293T cells [Lipo-gDNA(V)], or nothing [Lipo(V)] (H). Cells were analyzed 24 hours after treatment for CD86 and I-Ab expression by flow cytometry. (**I**) Wild-type mouse BMDCs were treated with LV generated from transient transfection or plasmid-free stable cell line and analyzed for CD86 expression by flow cytometry and for the amount of IL-12/23 and IL-6 in the supernatant by ELISA. Data are representative of three (A to F) or two (G to I) independent experiments. Results are shown as mean ± SEM (G to I). $P > 0.05$; $^{*}P < 0.05$; $^{**}P < 0.005$ (unpaired Student's *t* test).

was not inherently immunostimulatory but contributed to antigen delivery. Viral envelope–mediated fusion itself induced DC activation in a PI3K-dependent but STING- and type I IFN signaling–independent manner. Last, cellular DNA packaged from producer cells carried by particles activated the host STING and cGAS pathway.

Our results suggest that DCs were pseudotransduced in vivo and capable of stimulating antigen-specific immunity. Because of the transient and relatively low amount of antigen delivered compared with LV transduction, pseudotransduction has been considered an artifact (*23*, *24*), and LV transduction has been considered the underlying mechanism of antigen delivery and immune stimulation (*1*, *9*, *14*, *43*). However, we found that reverse-transcribed LV DNA was not inherently immunostimulatory in vivo but contributed to antigen delivery. This is consistent with our in vitro results showing that virtually all of the antigenic stimulation of DCs was due to pseudotransduction because activation was insensitive to RTIs and efficiently occurred with genome-deficient vectors. Neither the dual mechanisms of transduction and pseudotransduction nor the powerful role of pseudotransduction for delivering antigen and activating DCs in vivo has been appreciated. In this study, we presume that transducing and pseudotransducing particles contain the vector-encoded protein, but separation of these particles by size or density has been proven difficult.

Viral fusion by herpes VLPs has been found to activate DCs in a STING-dependent manner (*38*). We found that DC activation was, in part, a consequence of fusion induced between the vector and endosomal membranes but in a STING-independent manner. Furthermore, PI3K signaling was activated downstream of VSV-G viral fusion because fusion-defective VLPs failed to activate PI3K and LV fusion and transduction was PI3K-independent (*39*, *40*). In contrast, herpes entry and fusion are regulated by PI3K (*44*–*47*). Although PI3K is important in VSV-mediated type I IFN production via TLR4 (*48*), we did not find whether type I IFN or TLR4 signaling was required for LV-mediated DC activation or immunization. How PI3K is activated by VSV-G–mediated viral fusion and whether there are intermediary signaling molecules remain unknown.

We identified cellular DNA packaged from producer cells and carried by vector particles as the dominant activator of the STING and cGAS pathway. Nonviral DNA such as plasmid DNA has been found in LV particles and reported to activate plasmacytoid DCs in

an MyD88-dependent manner (*13*). However, the vast majority of DNA in our LV preparations was human genomic DNA. Further, LVs generated by plasmid-free cell lines capably activated immune responses (*41*, *42*). We did not examine plasmacytoid DCs because type I IFN signaling was not required for DC activation and pseudotransduction of plasmacytoid DCs was not detected in vivo. We assume that vector-encoded proteins such as GFP and OVA were merely encapsulated cytoplasm in the particles, but how genomic DNA is packaged within particles will require further investigation. HIV infection induces cell death by pyroptosis, a process that leads to DNA fragmentation (*49*). It could be that HIV particles pick up random fragmented DNA from the infected host cell. However, the formation of vector particles by transfection does not typically induce pyroptosis. Liposomal transfection reagents are added to dividing cells and may induce host DNA damage and increase cytosolic dsDNA in cells (*50*). Therefore, fragmented, cytoplasmic genomic DNA may be available for encapsulation in various cell types via different processes. We found that the human genomic DNA detected in our LV preparation randomly represented the human chromosomes. In addition, viral particles generated from at least two cell types packaged genomic DNA. Whether the incorporation of genomic DNA into vector particles extends to other viruses generated from different cell types remains to be determined.

In conclusion, we identify several important mechanisms involved in DC-targeted LV immunization. We highlight the importance of LV pseudotransduction as a mechanism of antigen delivery and immune stimulation in vivo. Our results suggest that viral fusion itself induces a PI3K-dependent, STING-independent process. In addition, the delivery of cellular DNA by viral particles activates the host STING and cGAS pathway. The development of DNA adjuvants as STING and cGAS agonists could provide new therapeutic strategies for vaccination.

MATERIALS AND METHODS

Study design

This study began as an investigation of understanding how LVs deliver antigen to DCs and provide immune stimulation. For this purpose, we used DCs in vitro and administered in vivo DC-targeted LVs to mice to study the effects of LV on DCs. We used various mechanistic studies involving VLPs and transgenic mice to determine the vector component and intracellular signaling pathway important to elicit DC activation. In mouse experiments, littermate comparisons were used when possible. All mice between 6 and 12 weeks of age were used with sex- and age-matched controls. The investigators were not blinded. In mouse experiments involving tumor injections, mice were euthanized when the tumor size reached 200 mm^2. Experimental replication is indicated in the figure legends.

Mice

C57BL/6J, MyD88$^{-/-}$, C57BL/6J-Ticam1^{Lps2}, Tmem173$^{-/-}$, C57BL/6-Tg(TcraTcrb)1100Mjb/J (the Jackson Laboratory), MAVS$^{-/-}$ (G. Cheng), and cGAS$^{-/-}$ (Z. Chen) mice were maintained on the C57BL/6J background and used according to the protocols approved by the Institutional Animal Care and Use Committee at California Institute of Technology (Caltech).

Isolation and culture of DCs

Differentiation of BMDCs was achieved by culture for 8 days in media containing GM-CSF (100 ng ml^{-1}) from J558L-conditioned medium (*2*). Human moDCs were generated by culture for 8 days of CD14$^+$ peripheral blood monocytes [University of California, Los Angeles (UCLA) Center for AIDS Research (CFAR) Virology Core Laboratory] in media containing human GM-CSF (100 ng ml^{-1}) and IL-4 (50 ng ml^{-1}; PeproTech). DCs were cultured in RPMI 1640 supplemented with 10% (v/v) fetal bovine serum (Sigma-Aldrich), 1% (v/v) nonessential amino acids (HyClone), 1 mM sodium pyruvate (Gibco), 10 mM Hepes (Gibco), and 0.05 mM 2-mercaptoethanol (Gibco). DCs were isolated ex vivo from mice using immunomagnetic negative isolation (table S1).

DC treatment with vectors

DCs (1×10^6 to 2×10^6 cells) were centrifuged with vectors at 1050*g* at 30°C for 90 min and with Polybrene (8 μg ml^{-1}). After centrifugation, the supernatant was removed and replaced with fresh medium and cytokines and incubated at 37°C with 5% CO_2. Cycloheximide and chloroquine (Sigma-Aldrich) were added to cell cultures 1 hour before vector treatment. Tenofovir and efavirenz [National Institutes of Health (NIH) AIDS Reagent Program] were added to cell cultures 6 hours before vector treatment.

Mouse immunization and tumor and RTI treatments

LVs and VLPs were injected subcutaneously into the right flank of mice. Prime-boost immunizations contained between 25 and 50 ng of p24. All vectors were normalized to equivalent amounts of OVA and/or p24 by ELISA. Unimmunized mice received equal volume of injections of phosphate-buffered saline (PBS). Blood samples were lysed with red blood cell lysis (BioLegend) before analysis. For the tumor experiments, mice received 5×10^6 EL4 or E.G7 cells injected subcutaneously into the opposing flanks of the mice. Tumor size was measured and shown as a product of the two largest perpendicular diameters $a \times b$ (in square millimeters). Tablets containing efavirenz (600 mg), emtricitabine (200 mg), and tenofovir disoproxil fumarate (300 mg; Cipla) were crushed, resuspended in PBS containing 1% (v/v) dimethyl sulfoxide, filtered through a 0.22-μm filter, and stored in aliquots at −80°C. RTIs were added to the fresh drinking water of mice containing efavirenz (10 mg ml^{-1}), emtricitabine (3.6 mg ml^{-1}), and tenofovir (5.4 mg ml^{-1}). Fresh water containing RTIs was replaced two times a week. Mice receiving no RTIs were given similar volumes of drinking water and replaced accordingly. Mice were initiated on RTIs 1 week before immunization and continued throughout the duration of the experiment.

In vitro DC stimulation of OT-1 cells

Mouse BMDCs were spin-infected with VLPs carrying OVA, washed, and resuspended in fresh media and lipopolysaccharide (LPS; 1 μg ml^{-1}). CD8$^+$ T cells were purified using MACS Columns (Miltenyi) from the spleen cells of OT-1 transgenic mice and cultured with the uninfected or VLP-infected BMDCs at a ratio of 1:1 and analyzed 24 hours after coculture.

Liposomes

Multilamellar liposomes were prepared using dioleoylphosphatidylcholine (DOPC), dioleoylphosphatidylglycerol (DOPG), and 1,2-dioleoyl-sn-glycero-3-phosphoethanolamine-*N*-[4-(p-maleimidophenyl) butyramide (MPB-PE) (NOF Corporation) and were combined in chloroform at a molar lipid ratio of DOPC/DOPG/MPB-PE = 4:1:5, and the organic solvent in the lipid mixture was evaporated under argon gas (*51*). The lipid mixture was further dried under vacuum overnight to form dried thin lipid films. The resultant dried film containing 1.12 μg of lipids was hydrated in bis-tris propane (10 mM) at pH 7.0 with GFP

(STA-201, Cell Biolabs) at a concentration of 125 ng ml^{-1} in a total volume of 300 µl. Polyhistidine-tagged VSV-G was expressed and purified from a suspension 293E cells after a 48-hour transfection using Ni-NTA column purification. Purified VSV-G protein (200 µg ml^{-1}) was added to the lipid hydration mixture before sonication. Alternatively, 5 ml of VSV-G–enveloped VLPs, collected from the medium of 293T cell transfected with pVSV-G and purified and concentrated as described above, was added to the lipid hydration mixture, as previously described (*37*), and DNA was not detectable by PCR in the liposomes made by this method. To add DNA into the liposomes, we extracted genomic DNA from 293T cells using a genomic DNA extraction kit (Thermo Fisher Scientific) or endotoxin-free intact plasmid DNA generated from *Escherichia coli* cells using a plasmid DNA extraction kit (Qiagen). Genomic or plasmid DNA (10 µg ml^{-1}) was added to the lipid hydration mixture. Lipid film and hydration mixture were vigorously vortexed every 10 min for 1 hour and then applied with four cycles of 15-s sonication (Misonix Microson XL2000) on ice in 1-min intervals for each cycle. To induce divalent-triggered vesicle fusion, we added $MgCl_2$ (10 mM). The resulting multilamellar vesicles were further cross-linked by the addition of dithiothreitol (1.5 mM; Sigma-Aldrich) for 1 hour at 37°C. The resulting vesicles were collected by centrifugation at 14,000*g* for 4 min and then washed twice with PBS and resuspended in PBS with a final DNA concentration of 250 ng $µl^{-1}$.

Statistical analyses

Data were analyzed using GraphPad Prism software (GraphPad Software Inc.). The statistical significance of differences for two groups was determined using Student's *t* test and one-way analysis of variance (ANOVA) for multiple comparisons, as indicated in the figure legends.

SUPPLEMENTARY MATERIALS

immunology.sciencemag.org/cgi/content/full/2/13/eaal1329/DC1
Materials and Methods
Fig. S1. Flow cytometry gating strategies.
Fig. S2. LV-mediated GFP expression and activation of BMDCs are dose-dependent.
Fig. S3. Mouse bone marrow–derived $CD11c^+CD11b^+$ cells are pseudotransduced and activated.
Fig. S4. Mouse cDCs are pseudotransduced in vivo.
Fig. S5. LV activation of DCs is independent of TLR4 and type I IFN signaling.
Fig. S6. Wild-type and mutant bone marrow–derived $CD11c^+CD11b^+$ cells are generated in GM-CSF culture.
Fig. S7. VSV-G viral fusion activates PI3K.
Fig. S8. Nonviral DNA in vector particle is primarily dsDNA, fragmented, and human genomic in origin.
Table S1. Antibodies used in this study.
Table S2. Primer sets used in this study.

REFERENCES AND NOTES

1. L. Yang, H. Yang, K. Rideout, T. Cho, K. i. Joo, L. Ziegler, A. Elliot, A. Walls, D. Yu, D. Baltimore, P. Wang, Engineered lentivector targeting of dendritic cells for in vivo immunization. *Nat. Biotechnol.* **26**, 326–334 (2008).
2. B. Dai, L. Yang, H. Yang, B. Hu, D. Baltimore, P. Wang, HIV-1 Gag-specific immunity induced by a lentivector-based vaccine directed to dendritic cells. *Proc. Natl. Acad. Sci. U.S.A.* **106**, 20382–20387 (2009).
3. N. Somaiah, M. S. Block, J. W. Kim, G. Shapiro, P. Hwu, J. P. Eder, R. L. Jones, S. Gnjatic, H. Lu, F. J. Hsu, S. Pollack, Phase I, first-in-human trial of LV305 in patients with advanced or metastatic cancer expressing NY-ESO-1. *J. Clin. Oncol.* **33**, 3021 (2015).
4. L. Bonifaz, D. Bonnyay, K. Mahnke, M. Rivera, M. C. Nussenzweig, R. M. Steinman, Efficient targeting of protein antigen to the dendritic cell receptor DEC-205 in the steady state leads to antigen presentation on major histocompatibility complex class I products and peripheral $CD8^+$ T cell tolerance. *J. Exp. Med.* **196**, 1627–1638 (2002).
5. D. P. Li, G. Romain, A.-L. Flamar, D. Duluc, M. Dullaers, X.-H. Li, S. Zurawski, N. Bosquet, A. K. Palucka, R. Le Grand, A. O'Garra, G. Zurawski, J. Banchereau, S. Oh, Targeting self- and foreign antigens to dendritic cells via DC-ASGPR generates IL-10–producing suppressive $CD4^+$ T cells. *J. Exp. Med.* **209**, 109–121 (2012).
6. N. Laguette, B. Sobhian, N. Casartelli, M. Ringeard, C. Chable-Bessia, E. Segeral, A. Yatim, S. Emiliani, O. Schwartz, M. Benkirane, SAMHD1 is the dendritic- and myeloid-cell-specific HIV-1 restriction factor counteracted by Vpx. *Nature* **474**, 654–657 (2011).
7. J. Dyall, J.-B. Latouche, S. Schnell, M. Sadelain, Lentivirus-transduced human monocyte-derived dendritic cells efficiently stimulate antigen-specific cytotoxic T lymphocytes. *Blood* **97**, 114–121 (2001).
8. K. Breckpot, P. Emeagi, M. Dullaers, A. Michiels, C. Heirman, K. Thielemans, Activation of immature monocyte-derived dendritic cells after transduction with high doses of lentiviral vectors. *Hum. Gene Ther.* **18**, 536–546 (2007).
9. F. Arce, H. M. Rowe, B. Chain, L. Lopes, M. K. Collins, Lentiviral vectors transduce proliferating dendritic cell precursors leading to persistent antigen presentation and immunization. *Mol. Ther.* **17**, 1643–1650 (2009).
10. G. Berger, C. Goujon, J.-L. Darlix, A. Cimarelli, SIV_{MAC} Vpx improves the transduction of dendritic cells with nonintegrative HIV-1-derived vectors. *Gene Ther.* **16**, 159–163 (2009).
11. A. Granelli-Piperno, L. Zhong, P. Haslett, J. Jacobson, R. M. Steinman, Dendritic cells, infected with vesicular stomatitis virus-pseudotyped HIV-1, present viral antigens to $CD4^+$ and $CD8^+$ T cells from HIV-1-infected individuals. *J. Immunol.* **165**, 6620–6626 (2000).
12. A.-S. Beignon, K. McKenna, M. Skoberne, O. Manches, I. DaSilva, D. G. Kavanagh, M. Larsson, R. J. Gorelick, J. D. Lifson, N. Bhardwaj, Endocytosis of HIV-1 activates plasmacytoid dendritic cells via Toll-like receptor–viral RNA interactions. *J. Clin. Invest.* **115**, 3265–3275 (2005).
13. A. Pichlmair, S. S. Diebold, S. Gschmeissner, Y. Takeuchi, Y. Ikeda, M. K. Collins, C. Reis e Sousa, Tubulovesicular structures within vesicular stomatitis virus G protein-pseudotyped lentiviral vector preparations carry DNA and stimulate antiviral responses via Toll-like receptor 9. *J. Virol.* **81**, 539–547 (2007).
14. K. Breckpot, D. Escors, F. Arce, L. Lopes, K. Karwacz, S. Van Lint, M. Keyaerts, M. Collins, HIV-1 lentiviral vector immunogenicity is mediated by Toll-like receptor 3 (TLR3) and TLR7. *J. Virol.* **84**, 5627–5636 (2010).
15. R. K. Berg, J. Melchjorsen, J. Rintahaka, E. Diget, S. Søby, K. A. Horan, R. J. Gorelick, S. Matikainen, C. S. Larsen, L. Ostergaard, S. R. Paludan, T. H. Mogensen, Genomic HIV RNA induces innate immune responses through RIG-I-dependent sensing of secondary-structured RNA. *PLOS ONE* **7**, e29291 (2012).
16. M. R. Jakobsen, R. O. Bak, A. Andersen, R. K. Berg, S. B. Jensen, J. Tengchuan, A. Laustsen, K. Hansen, L. Østergaard, K. A. Fitzgerald, T. S. Xiao, J. G. Mikkelsen, T. H. Mogensen, S. R. Paludan, IFI16 senses DNA forms of the lentiviral replication cycle and controls HIV-1 replication. *Proc. Natl. Acad. Sci. U.S.A.* **110**, E4571–E4580 (2013).
17. D. Gao, J. Wu, Y.-T. Wu, F. Du, C. Aroh, N. Yan, L. Sun, Z. J. Chen, Cyclic GMP-AMP synthase is an innate immune sensor of HIV and other retroviruses. *Science* **341**, 903–906 (2013).
18. X. Lahaye, T. Satoh, M. Gentili, S. Cerboni, C. Conrad, I. Hurbain, A. El Marjou, C. Lacabaratz, J.-D. Lelièvre, N. Manel, The capsids of HIV-1 and HIV-2 determine immune detection of the viral cDNA by the innate sensor cGAS in dendritic cells. *Immunity* **39**, 1132–1142 (2013).
19. L. Deml, C. Speth, M. P. Dierich, H. Wolf, R. Wagner, Recombinant HIV-1 $Pr55^{gag}$ virus-like particles: Potent stimulators of innate and acquired immune responses. *Mol. Immunol.* **42**, 259–277 (2005).
20. S. Kuate, C. Stahl-Hennig, H. Stoiber, G. Nchinda, A. Floto, M. Franz, U. Sauermann, S. Bredl, L. Deml, R. Ignatius, S. Norley, P. Racz, K. Tenner-Racz, R. M. Steinman, R. Wagner, K. Überla, Immunogenicity and efficacy of immunodeficiency virus-like particles pseudotyped with the G protein of vesicular stomatitis virus. *Virology* **351**, 133–144 (2006).
21. L. Buonaguro, M. L. Tornesello, M. Tagliamonte, R. C. Gallo, L. X. Wang, R. Kamin-Lewis, S. Abdelwahab, G. K. Lewis, F. M. Buonaguro, Baculovirus-derived human immunodeficiency virus type 1 virus-like particles activate dendritic cells and induce ex vivo T-cell responses. *J. Virol.* **80**, 9134–9143 (2006).
22. S. R. Beaty, C. E. Rose Jr., S.-s. J. Sung, Diverse and potent chemokine production by lung $CD11b^{high}$ dendritic cells in homeostasis and in allergic lung inflammation. *J. Immunol.* **178**, 1882–1895 (2007).
23. D. L. Haas, S. S. Case, G. M. Crooks, D. B. Kohn, Critical factors influencing stable transduction of human $CD34^+$ cells with HIV-1-derived lentiviral vectors. *Mol. Ther.* **2**, 71–80 (2000).
24. K. L. Nash, A. M. L. Lever, Green fluorescent protein: Green cells do not always indicate gene expression. *Gene Ther.* **11**, 882–883 (2004).
25. P.-E. Mangeot, S. Dollet, M. Girard, C. Ciancia, S. Joly, M. Peschanski, V. Lotteau, Protein transfer into human cells by VSV-G-induced nanovesicles. *Mol. Ther.* **19**, 1656–1666 (2011).
26. J. M. Odegard, B. Kelley-Clarke, S. U. Tareen, D. J. Campbell, P. A. Flynn, C. J. Nicolai, M. M. Slough, C. D. Vin, P. J. McGowan, L. T. Nelson, J. Ter Meulen, T. W. Dubensky Jr., S. H. Robbins, Virological and preclinical characterization of a dendritic cell targeting,

integration-deficient lentiviral vector for cancer immunotherapy. *J. Immunother.* **38**, 41–53 (2015).
27. T. C. Albershardt, D. J. Campbell, A. J. Parsons, M. M. Slough, J. ter Meulen, P. Berglund, LV305, a dendritic cell-targeting integration-deficient ZVex^{TM}-based lentiviral vector encoding NY-ESO-1, induces potent anti-tumor immune response. *Mol. Ther. Oncolytics* **3**, 16010 (2016).
28. O. Adachi, T. Kawai, K. Takeda, M. Matsumoto, H. Tsutsui, M. Sakagami, K. Nakanishi, S. Akira, Targeted disruption of the *MyD88* gene results in loss of IL-1- and IL-18-mediated function. *Immunity* **9**, 143–150 (1998).
29. M. Yamamoto, S. Sato, H. Hemmi, K. Hoshino, T. Kaisho, H. Sanjo, O. Takeuchi, M. Sugiyama, M. Okabe, K. Takeda, S. Akira, Role of adaptor TRIF in the MyD88-independent Toll-like receptor signaling pathway. *Science* **301**, 640–643 (2003).
30. H. Kato, O. Takeuchi, S. Sato, M. Yoneyama, M. Yamamoto, K. Matsui, S. Uematsu, A. Jung, T. Kawai, K. J. Ishii, O. Yamaguchi, K. Otsu, T. Tsujimura, C.-S. Koh, C. R. E. Sousa, Y. Matsuura, T. Fujita, S. Akira, Differential roles of MDA5 and RIG-I helicases in the recognition of RNA viruses. *Nature* **441**, 101–105 (2006).
31. U. Muller, U. Steinhoff, L. F. L. Reis, S. Hemmi, J. Pavlovic, R. M. Zinkernagel, M. Aguet, Functional-role of type-I and type-II interferons in antiviral defense. *Science* **264**, 1918–1921 (1994).
32. H. Ishikawa, G. N. Barber, Sting is an endoplasmic reticulum adaptor that facilitates innate immune signaling. *Cytokine* **48**, 128 (2009).
33. X.-D. Li, J. Wu, D. Gao, H. Wang, L. Sun, Z. J. Chen, Pivotal roles of cGAS-cGAMP signaling in antiviral defense and immune adjuvant effects. *Science* **341**, 1390–1394 (2013).
34. R. Z. Florkiewicz, J. K. Rose, A cell line expressing vesicular stomatitis virus glycoprotein fuses at low pH. *Science* **225**, 721–723 (1984).
35. J. M. Smit, R. Bittman, J. Wilschut, Low-pH-dependent fusion of Sindbis virus with receptor-free cholesterol- and sphingolipid-containing liposomes. *J. Virol.* **73**, 8476–8484 (1999).
36. L. Zhang, H. P. Ghosh, Characterization of the putative fusogenic domain in vesicular stomatitis virus glycoprotein G. *J. Virol.* **68**, 2186–2193 (1994).
37. A. Abe, A. Miyanohara, T. Friedmann, Enhanced gene transfer with fusogenic liposomes containing vesicular stomatitis virus G glycoprotein. *J. Virol.* **72**, 6159 (1998).
38. C. K. Holm, S. B. Jensen, M. R. Jakobsen, N. Cheshenko, K. A. Horan, H. B. Moeller, R. Gonzalez-Dosal, S. B. Rasmussen, M. H. Christensen, T. O. Yarovinsky, F. J. Rixon, B. C. Herold, K. A. Fitzgerald, S. R. Paludan, Virus-cell fusion as a trigger of innate immunity dependent on the adaptor STING. *Nat. Immunol.* **13**, 737–743 (2012).
39. E. F. Dunn, R. Fearns, J. H. Connor, Akt inhibitor Akt-IV blocks virus replication through an Akt-independent mechanism. *J. Virol.* **83**, 11665–11672 (2009).
40. M. F. Saeed, A. A. Kolokoltsov, A. N. Freiberg, M. R. Holbrook, R. A. Davey, Phosphoinositide-3 kinase-Akt pathway controls cellular entry of Ebola virus. *PLOS Pathog.* **4**, e1000141 (2008).
41. C.-L. Lee, M. Chou, B. Dai, L. Xiao, P. Wang, Construction of stable producer cells to make high-titer lentiviral vectors for dendritic cell-based vaccination. *Biotechnol. Bioeng.* **109**, 1551–1560 (2012).
42. P. D. Bryson, C. Zhang, C.-L. Lee, P. Wang, A tetracycline-regulated cell line produces high-titer lentiviral vectors that specifically target dendritic cells. *J. Vis. Exp.* **76**, e50606 (2013).
43. C. Esslinger, L. Chapatte, D. Finke, I. Miconnet, P. Guillaume, F. Lévy, H. R. MacDonald, In vivo administration of a lentiviral vaccine targets DCs and induces efficient CD8$^+$ T cell responses. *J. Clin. Invest.* **111**, 1673–1681 (2003).
44. V. Tiwari, D. Shukla, Phosphoinositide 3 kinase signalling may affect multiple steps during herpes simplex virus type-1 entry. *J. Gen. Virol.* **91**, 3002–3009 (2010).
45. I. J. MacLeod, T. Minson, Binding of herpes simplex virus type-1 virions leads to the induction of intracellular signalling in the absence of virus entry. *PLOS ONE* **5**, e9560 (2010).
46. N. Cheshenko, HSV activates Akt to trigger calcium release and promote viral entry: Novel candidate target for treatment and suppression (vol 27, pg 2584, 2013). *Faseb J.* **29**, 355 (2015).
47. A. V. Nicola, S. E. Straus, Cellular and viral requirements for rapid endocytic entry of herpes simplex virus. *J. Virol.* **78**, 7508–7517 (2004).
48. G. Schabbauer, J. Luyendyk, K. Crozat, Z. Jiang, N. Mackman, S. Bahram, P. Georgel, TLR4/CD14-mediated PI3K activation is an essential component of interferon-dependent VSV resistance in macrophages. *Mol. Immunol.* **45**, 2790–2796 (2008).
49. G. Doitsh, N. L. K. Galloway, X. Geng, Z. Yang, K. M. Monroe, O. Zepeda, P. W. Hunt, H. Hatano, S. Sowinski, I. Muñoz-Arias, W. C. Greene, Cell death by pyroptosis drives CD4 T-cell depletion in HIV-1 infection. *Nature* **505**, 509–514 (2014).
50. K. B. Knudsen, H. Northeved, P. E. Kumar, A. Permin, T. Gjetting, T. L. Andresen, S. Larsen, K. M. Wegener, J. Lykkesfeldt, K. Jantzen, S. Loft, P. Møller, M. Roursgaard, In vivo toxicity of cationic micelles and liposomes. *Nanomedicine* **11**, 467–477 (2015).
51. Y. Liu, J. Fang, K.-I. Joo, M. K. Wong, P. Wang, Codelivery of chemotherapeutics via crosslinked multilamellar liposomal vesicles to overcome multidrug resistance in tumor. *PLOS ONE* **9**, e110611 (2014).

Acknowledgments: We thank G. Cheng (UCLA) for the MAVS$^{-/-}$ mice, Z. Chen (University of Texas Southwestern Medical Center) for the cGAS$^{-/-}$ mice, the UCLA/CFAR Virology Core Laboratory (5P30 AI028697), the UCLA Specialty Training and Advanced Research Program, the AIDS Reagent Program, the National Institute of Allergy and Infectious Diseases Tetramer Core Facility, the UCLA/CFAR Virology Core Laboratory, and the PrimerBank. This work was supported by the Millard and Muriel Jacobs Genetics and Genomics Laboratory at Caltech. We thank M. Bethune and G. Li for the review of the manuscript. **Funding:** This work was supported by the NIH (OPPGH5157) and the American Foundation for AIDS Research (108292-51-RGRL). J.T.K. was supported by the NIH (KL2TR001882) and the UCLA Specialty Training and Advanced Research (STAR) Program. **Author contributions:** J.T.K. designed the research, performed the experiments, analyzed the results, and drafted the manuscript. Y.L., B.D., G.L., R.P.K., K.K.L., and Y.O. performed the experiments. L.Y. and P.W. discussed the results and drafted the manuscript. D.B. designed the research, discussed the results, drafted the manuscript, and provided financial support. **Competing interests:** P.W., L.Y., and D.B. are inventors on issued patents for DC-targeted lentiviral technology discussed in this study, which has been licensed to Immune Design Corporation (IDC), and are stock holders in IDC. D.B. is also a member of Board of Directors of IDC. **Data and materials availability:** DNA sequence data have been deposited in Sequence Read Archive under accession number SAMN07195639.

Submitted 30 September 2016
Resubmitted 14 March 2017
Accepted 12 June 2017
Published 21 July 2017
10.1126/sciimmunol.aal1329

Citation: J. T. Kim, Y. Liu, R. P. Kulkarni, K. K. Lee, B. Dai, G. Lovely, Y. Ouyang, P. Wang, L. Yang, D. Baltimore, Dendritic cell–targeted lentiviral vector immunization uses pseudotransduction and DNA-mediated STING and cGAS activation. *Sci. Immunol.* **2**, eaal1329 (2017).

Science Immunology

Dendritic cell–targeted lentiviral vector immunization uses pseudotransduction and DNA-mediated STING and cGAS activation

Jocelyn T. Kim, Yarong Liu, Rajan P. Kulkarni, Kevin K. Lee, Bingbing Dai, Geoffrey Lovely, Yong Ouyang, Pin Wang, Lili Yang and David Baltimore

Sci. Immunol. **2**, eaal1329.
DOI: 10.1126/sciimmunol.aal1329

Successful vaccination through "pseudo" science

Successful vaccines need to deliver antigen as well as stimulate the immune response. Kim *et al*. examine the mechanisms by which dendritic cell (DC)–targeting lentiviral vectors (LVs) accomplish both of these goals. They found that transduction was not required and that pseudotransduction was sufficient for antigen delivery and immune stimulation. The authors identified two mechanisms behind this effect: Viral fusion induced a PI3K-dependent immune stimulation pathway, and human genomic DNA within the virion preparations activated the STING/cGAS pathway. These data suggest that STING and cGAS agonists could serve as potential vaccine adjuvants.

Science Immunology

immunology.sciencemag.org/cgi/content/full/2/13/eaal1329/DC1

Supplementary Materials for

Dendritic cell–targeted lentiviral vector immunization uses pseudotransduction and DNA-mediated STING and cGAS activation

Jocelyn T. Kim, Yarong Liu, Rajan P. Kulkarni, Kevin K. Lee, Bingbing Dai, Geoffrey Lovely, Yong Ouyang, Pin Wang, Lili Yang, David Baltimore*

*Corresponding author. Email: baltimo@caltech.edu

Published 21 July 2017, *Sci. Immunol.* **2**, eaal1329 (2017)
DOI: 10.1126/sciimmunol.aal1329

This PDF file includes:

Materials and Methods

Antibodies and flow cytometry. Cells were stained with appropriate antibodies (Table S1) and analyzed on a MACSQuant analyzer (Miltenyi) using FlowJo software (TreeStar) with appropriate gating strategies (fig. S1). For dead cell staining, propidium iodine 1 μg ml^{-1} was added.

Cell lines. HEK293T/17 cells (ATCC) and 293T.DCSIGN cells (*1*) were cultured in DMEM with 10% (vol/vol) FBS. EL4 (C57BL/6J, H-2^b, thymoma) and E.G7 (derived from EL4 cells stably expressing one copy of chicken OVA cDNA) provided by L. Yang (UCLA) and GXR.CEM human lymphoblastoid $CD4^+$ T cells provided by B. Walker (Ragon Institute) were cultured in RPMI-1640 medium with 10% (vol/vol) FBS. All media was supplemented with 1% (vol/vol) penicillin and streptomycin (Gibco).

LV, VLP, and infectious HIV-1 production. A third generation HIV-based LV system was used with transfer vectors: FUGW encoding GFP (*1*) or FOVA encoding an invariant chain-OVA fusion construct (*72*). The packaging plasmids pMDLg/pRRE encoded *gag* and *pol* and pRSV-Rev encoded *rev*. The envelope plasmids were pVSV-G and pSVGmu (*1*). Introducing mutations G124A and P127A generated the fusion-defective VSV-G (*46*). The plasmid pNL4-3 (NIH AIDS Reagent Program) encoded infectious HIV-1. 293T cells were transfected using BioT (Bioland Scientific) according to manufacturer's instructions. To generate VLPs the LV transfer vector plasmid was omitted. Omitting the packaging plasmids generated capsid deficient vectors. Transfecting with the packaging plasmids generated bald particles (*7*). To generate VLPs carrying GFP or OVA, an expression plasmid encoding GFP (p.GFP) or p.OVA was included during transfection. Puc19 plasmid was transfected into 293T cells as a negative control. All viral supernatants were harvested at 36, 48, and 60 h post-transfection and filtered

through a 0.45-μm filter. The cell-free LV and VLP supernatants were additionally ultracentrifugated (Optima L-80 K preparative ultracentrifuge, Beckman Coulter) at 80,000 *g* for 90 min through a 20% (vol/vol) sucrose cushion. The pellets were then resuspended in an appropriate volume of cold PBS.

Quantification of vectors. 293T and 293T.DCSIGN cells were infected with LV and polybrene 5 μg ml^{-1} and analyzed at 48 h for GFP expression by flow cytometry to determine the infectious titer by the dilution ranges that exhibited a linear response. The concentration of gag was measured by p24 capture ELISA Kit (ImmunoDiagnostics) and GFP by GFP ELISA Kit (Abcam). The concentration of iOVA was determined using a sandwich ELISA with for coating onto 96-well plates using anti-CD74 5 μg ml^{-1} for coating of plates. The vectors were lysed in 0.5% (vol/vol) Triton X-100 and incubated on coated plates. The amount of captured OVA was determined using anti-chicken OVA 5 μg ml^{-1} and a horseradish peroxidase-conjugated goat-anti-mouse IgG (Bethyl Lab) at a dilution of 1:10,000. TMB Peroxidase Substrate System (KPL) was used and absorbance read at 450 nm.

Immunoblot analysis. Vector preparations were lysed in 1% Triton X-100 in PBS supplemented with HALT protease and phosphatase inhibitor cocktail (Life Technologies) and clarified by centrifugation. Aliquots of the lysate were mixed with non-reduced Laemmli's sample buffer and were resolved by 5–15% (wt/vol) SDS-PAGE. Antibodies to GFP, OVA, VSVG, and p24 were used (Table S1). To determine if proteins were inside the vector particles, samples were pre-treated with proteinase K 10 μg ml^{-1} (Qiagen) and incubated at 55 °C for 1 h, then the proteinase K was inactivated with PMSF 1mM (Sigma) before samples were lysed.

Fluorescent imaging. Cells were washed once with PBS, fixed using 4% (vol/vol) paraformaldehyde in PBS (10 min at 22 °C), and washed 4 times with PBS. Images were

collected using a fluorescence microscope (Axiovert 200m; Zeiss) equipped with three filter wheels (Lambda 10-3; Sutter Instruments), and a CCD camera (Evolution/Qimaging; Media Cybernetics). Images were collected using Image-ProPlus 5.1 software (Media Cybernetics). All data within each experiment was collected at identical imaging settings; relevant sets of images were adjusted only for brightness/contrast.

DNA analysis by PCR and fluoremetry. Virus and VLP samples were inactivated/lysed by heating to 95 °C for 15 min. To determine whether DNA was carried within the particles, virus and VLP samples were pre-treated with DNase I (Sigma) at a final concentration of 0.1 mg ml^{-1} at room temperature for 10 min, and then the DNase I was inactivated with EDTA 0.625 mM at 70 °C for 10 min, before inactivation/lysis. To show that DNase I degradation was complete, DNase I was not inactivated by EDTA prior to lysis. PCR amplifications from samples were carried out in 0.2-mL thin-walled reaction vessels in the Eppendorf Mastercycler proS. REDExtract-N-Amp PCR ReadyMix (Sigma) was used per manufacturer instructions to obtain readily visible PCR products after 35 amplification cycles (30 s at 95 °C, 30 s at 50 °C and 1 min at 72 °C) with the appropriate primer sequences **(**Table S2**)**. The amplification products were electrophoresed on 2% (wt/vol) agarose gel with subsequent ethidium bromide staining. DNA from vector preparation was extracted using a genomic DNA extraction kit (ThermoFisher Scientific). Double-stranded and single-stranded DNA was measured from extracted DNA using the Quantifluor dsDNA and ssDNA system (Promega).

DNA deep sequencing. Total DNA from 200 µl of vector preparation was fragmented using Qsonica Q800R sonicator to the average size of ~200 bp, the fragments were end repaired and A-tailed, followed by adaptor ligation and PCR. DNA libraries were constructed using the Nextera XT DNA Sample Preparation Kit and Nextera XT Index Kit (Illumina). Libraries were

quantified with Quibit and the insert size distribution was assessed with 2100 BioAnalyzer (Agilent). All libraries were sequenced on Illumina HiSeq2500. Reads were aligned to the human genome version hg19 and the plasmid DNA sequence maps using BWA.

HIV passaging. Human PBMCs (UCLA Center for AIDS Research Virology Core Lab) were cultured in PHA 5 μg ml^{-1} (Sigma) with IL-2 5 ng ml^{-1} (Peprotech) cells at 1×10^6 cells ml^{-1} and infected with NL4-3 virus supernatant (50 ng p24) and incubated at 37 °C for 1 d. Infected cells were washed and incubated again at 37 °C for 2 d. Uninfected cells were concurrently treated in an identical manner. Cell-free supernatant was collected and filtered through a 0.22 μm filter. Aliquots of cell-free supernatants were stored at –80 °C.

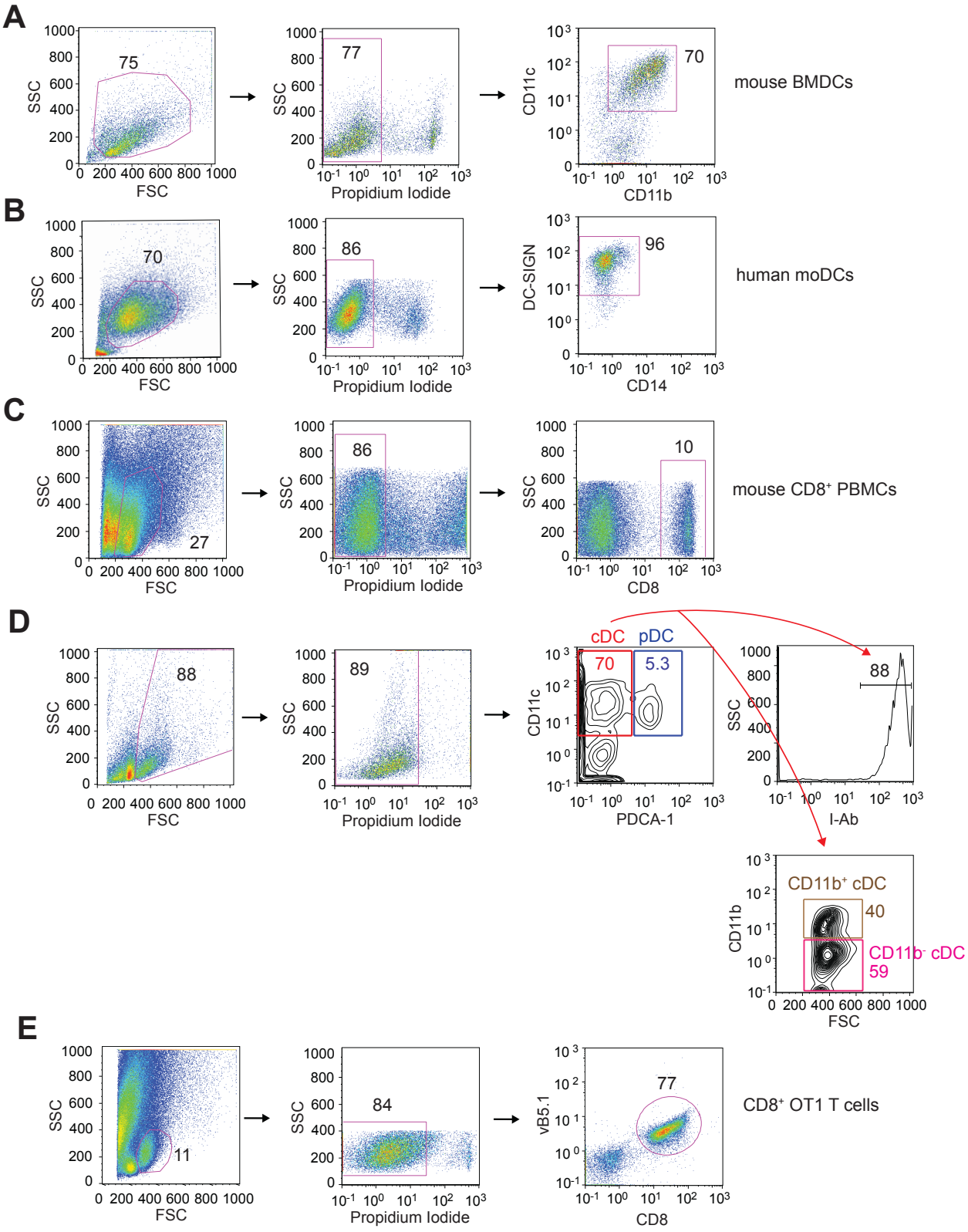

Fig. S1. Flow cytometry gating strategies. (**A-E**) Flow cytometric analysis of mouse BMDCs (A), human moDCs (B), mouse CD8$^+$ PBMCs (C), mouse DCs isolated from lymph nodes (D), and mouse CD8$^+$ OT1 T cells (E). Numbers adjacent to the gates reflect the percentage of cells within the gates.

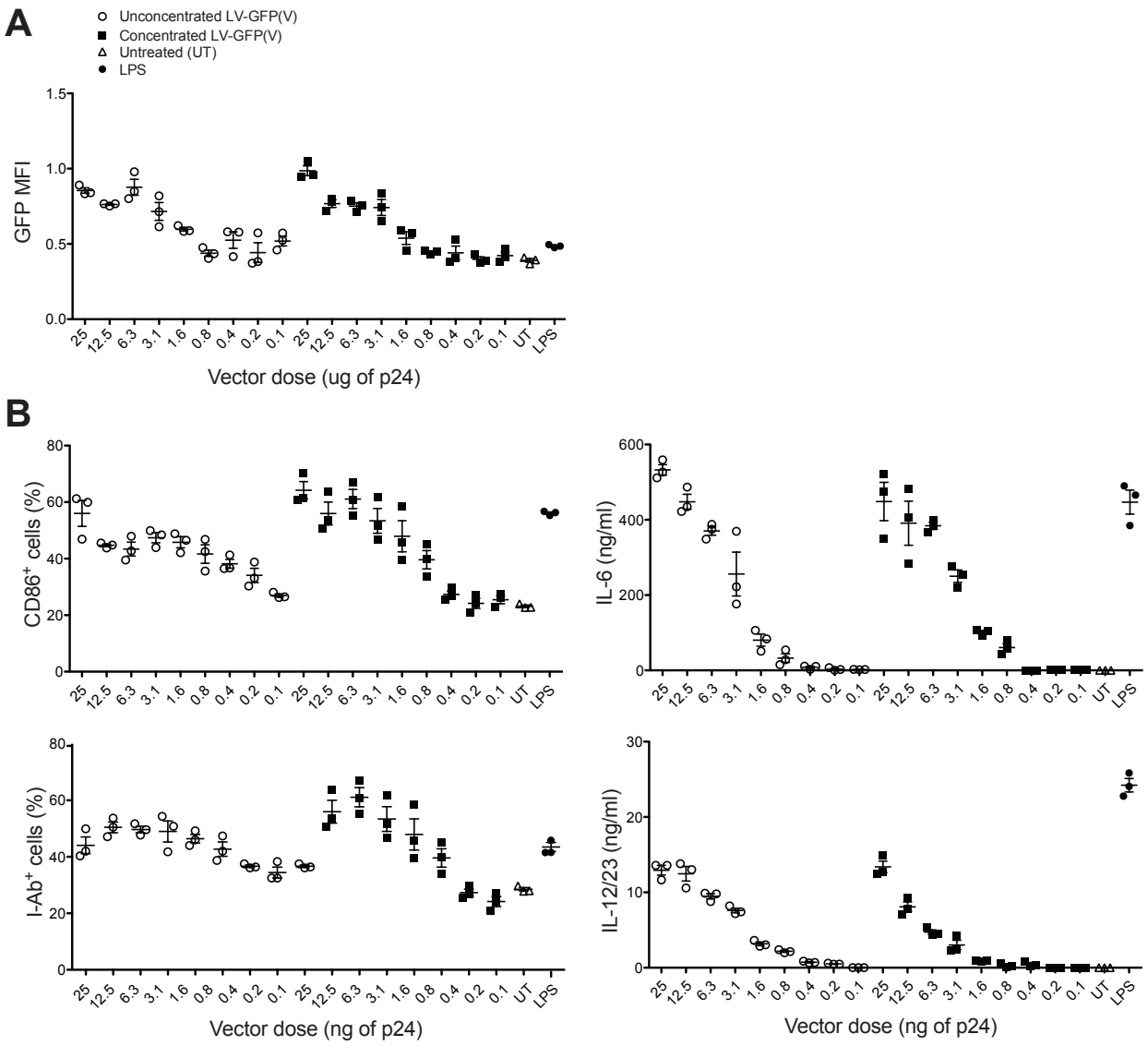

Fig. S2. LV-mediated GFP expression and activation of BMDCs are dose-dependent. BMDCs (2E6 cells/ml) were treated with serial dilutions of LV-GFP(V) in 600ul total volume. (**A**) Expression of GFP by BMCDs was measured by flow cytometry 24 h post-LV treatment. (**B**) The percentages of $CD86^+$ and $I\text{-}Ab^+$ cells was measured by flow cytometry and cytokine secretion of IL-6 and IL-12/23 in the supernatant at 24 h post-LV

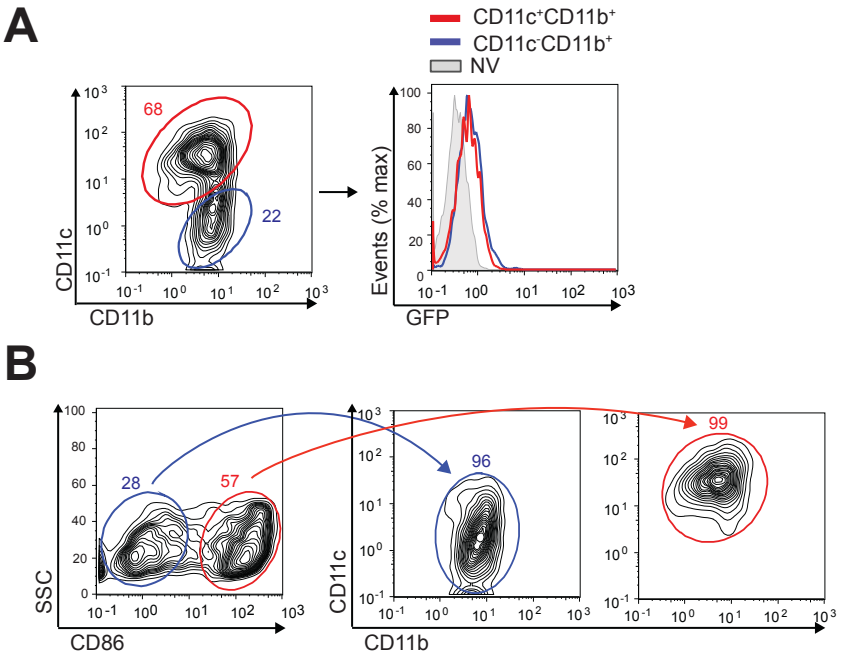

Fig. S3. Mouse bone marrow-derived CD11c$^+$CD11b$^+$ cells are pseudotransduced and activated. (**A, B**) Bone marrow cells from wild-type mouse were cultured in GM-GSF for 8 days and treated with LV-GFP(V) and analyzed by flow cytometry 24 h post-LV treatment. FACS plot showing CD11c and CD11b expression of cells (A, left). FACS histogram showing GFP expression of the gated CD11c$^+$CD11b$^+$ and CD11c$^-$CD11b$^+$ populations (A, right). Cells were then gated based on expression of activation marker CD86 (B, left). CD86$^+$ and CD86$^-$ were analyzed for expression of CD11c and CD11b (B, right).

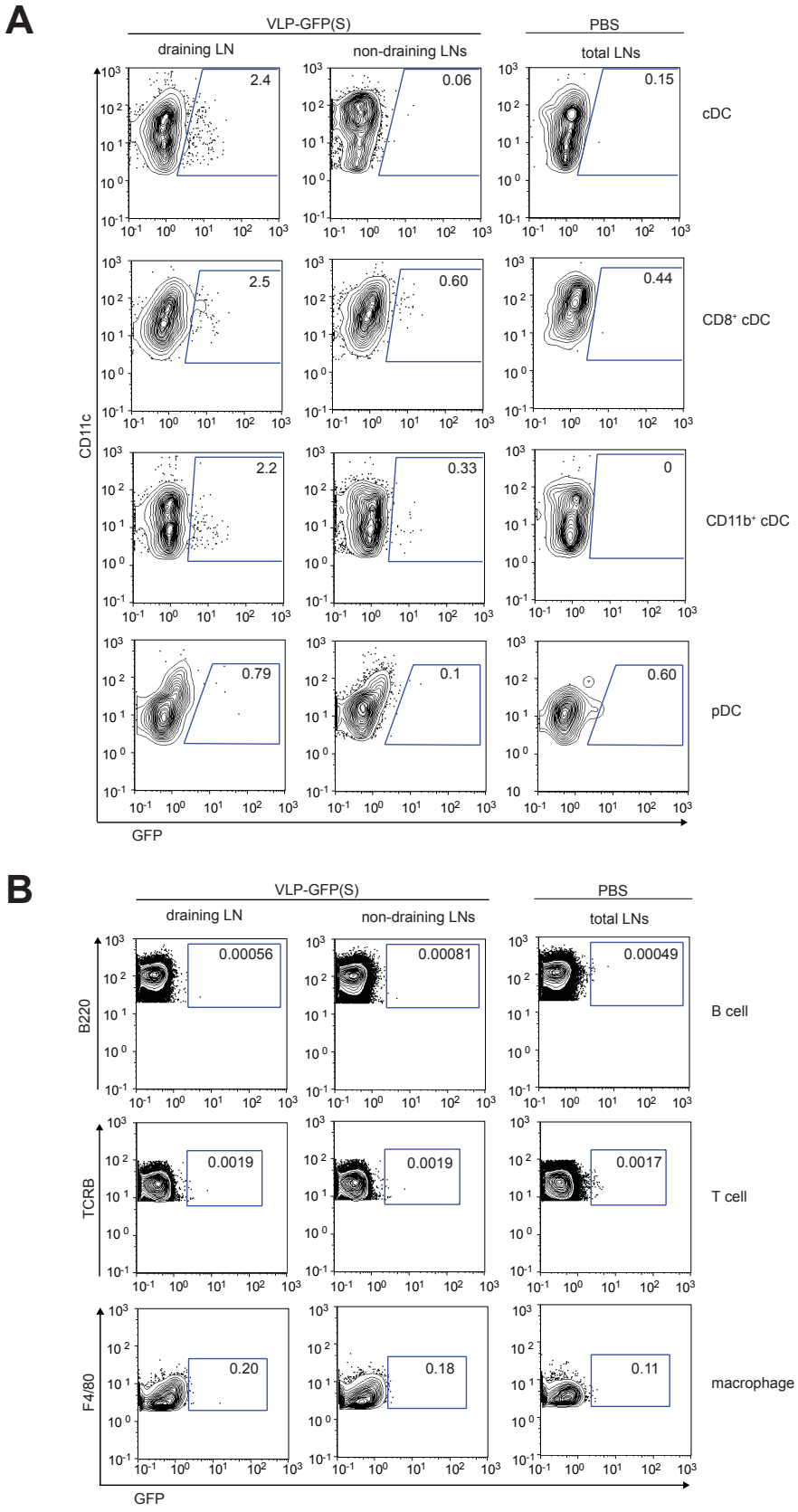

Fig. S4. Mouse cDCs are pseudotransduced *in vivo*. VLP carrying GFP pseudotyped with SVGmu (100ng of p24) was injected subcutaenously into the R hindleg of wild-type mice. Control mice received equal volumes of PBS. Right inguinal draining lymph node and non-draining lymph nodess (left inguinal, axillary, and cervical) were harvested 24 h post-injection. (**A**) DC subsets were gated (fig. S1D) and analyzed for GFP expression. (**B**) B cells, T cells, and macrophages isolated from lymph nodes were also analzyed for GFP expression.

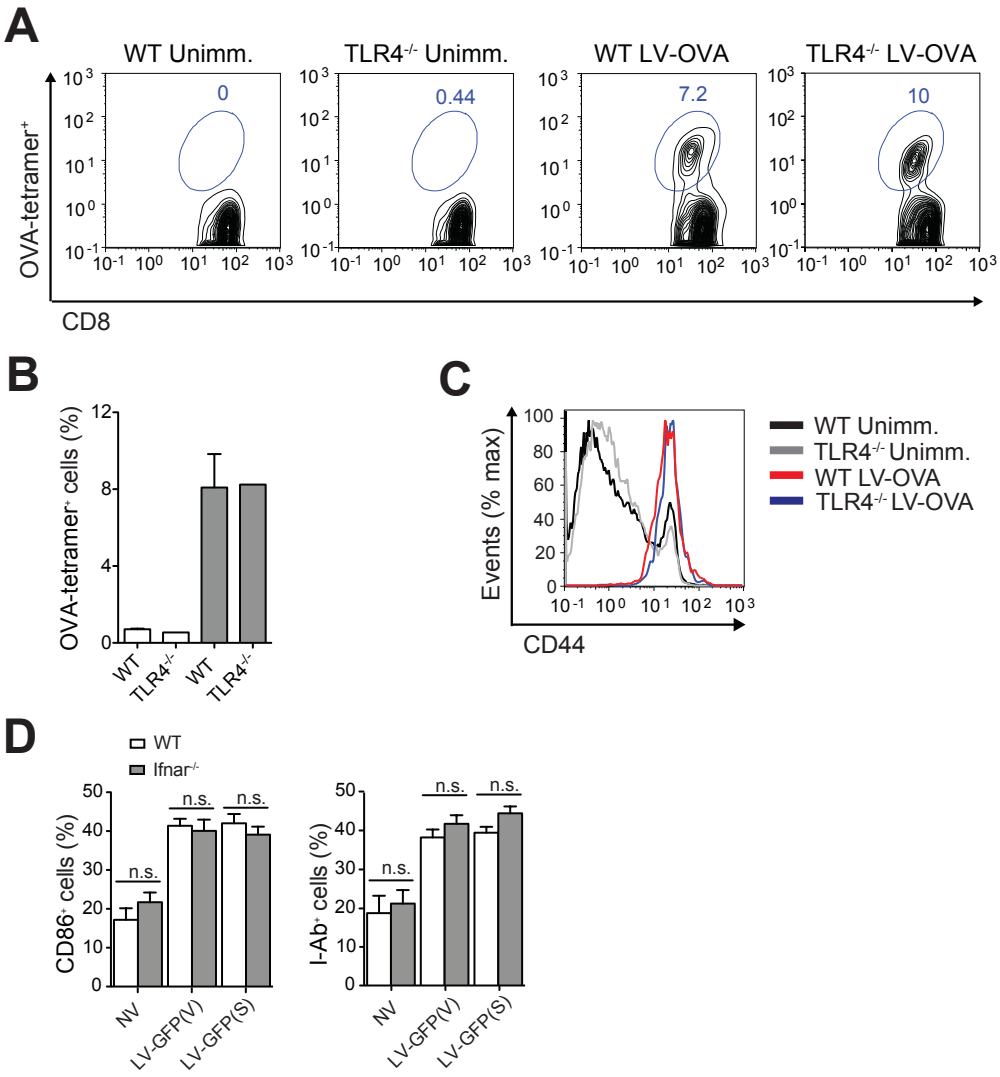

Fig. S5. LV activation of DCs is independent of TLR4 and type I IFN signaling. (**A-C**) TLR4$^{-/-}$ (n=2) and wild-type mice (n=4) were immunized with DC-targeting LV-OVA. Unimminzed TLR4$^{-/-}$ (n=2) and wild-type mice (n=4) received equal volumes of PBS. Two week post-immunization, spleens were harvested and CD8^{+} T cells analyzed by flow cytometry. FACS plots showing OVA-tetramer expression of CD8^{+} T cells (A). Graph depicts percentages of OVA-tetramer^{+} CD8^{+} T cells from the spleen of immunized and unimmunized mice (B). FACS histogram plot show CD44 expression of OVA-tetramer^{+}CD8^{+} T cells from immunized mice and naive CD8^{+} T cells from unimmunized mice (C). (**D**) BMDCs from mice deficient in Type I IFN receptor were treated with LV-GFP(V) or LV-GFP(S) and analyzed at 24 h for expression of CD86 and I-Ab by flow cytometry. n.s.=not significant, $P > 0.05$; (unpaired Student's t-test).

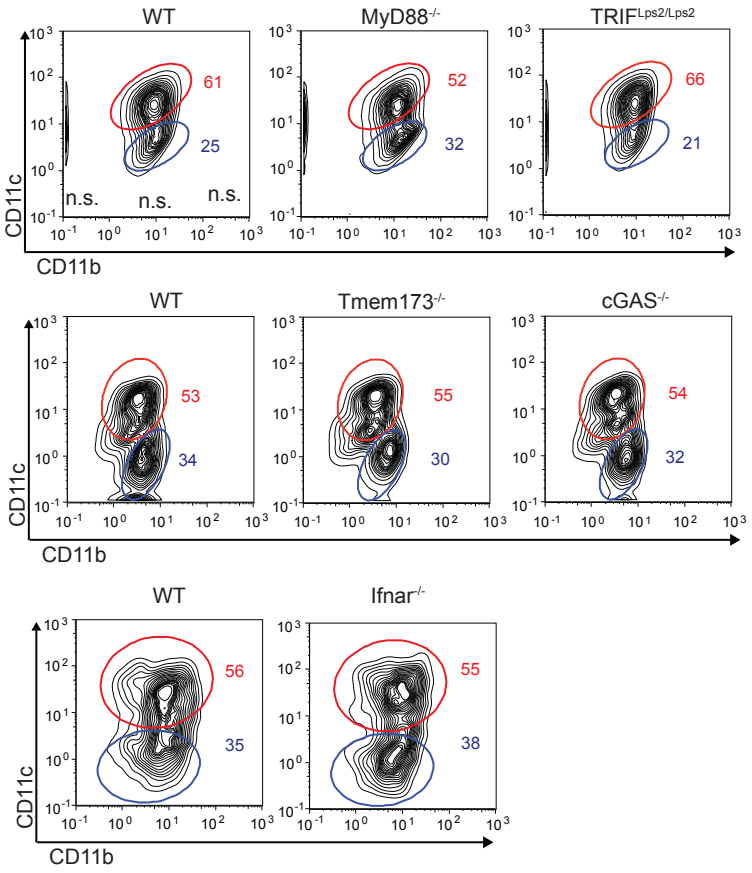

Fig. S6. Wild-type and mutant bone marrow-derived CD11c^{+}CD11b^{+} cells are generated in GM-CSF culture. Bone marrow cells from wild-type and mutant mice were cultured in 100ng ml^{-1} GM-CSF for 8 days. FACS plot showing CD11c and CD11b expression of these BM-derived cells.

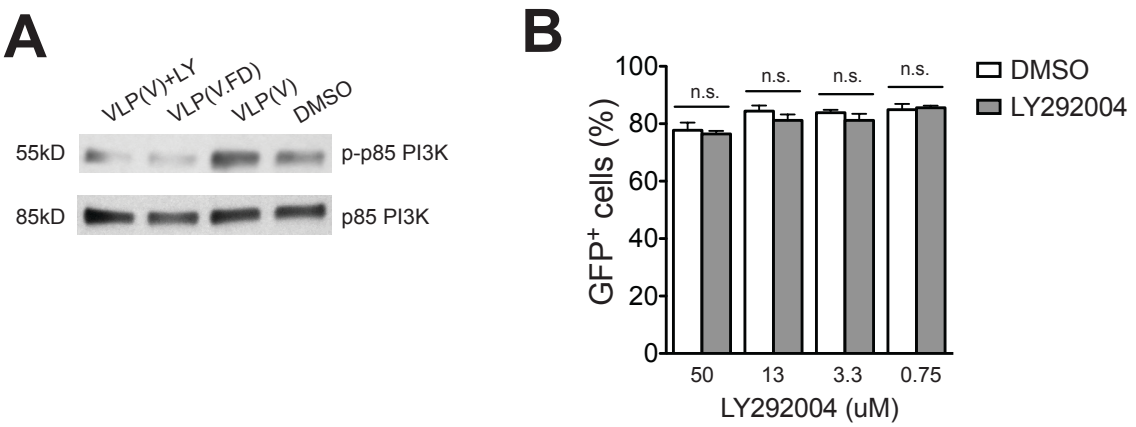

Fig. S7. VSV-G viral fusion activates PI3K. (**A**) Wild-type BMDCs were treated with VLP(V) with or without 50uM LY292004 or fusion defective VLP(V.FD) and analyzed at 2.5 h by Western blot for phosphorylated p85 subunit of PI3K and total p85. (**B**) 293T cells were incubated with LY2902004 1 h prior to treatment with LV-GFP(V) and then analyzed 48 h later for GFP expression by flow cytometry. n.s.=not significant, $P > 0.05$; (unpaired Student's t-test).

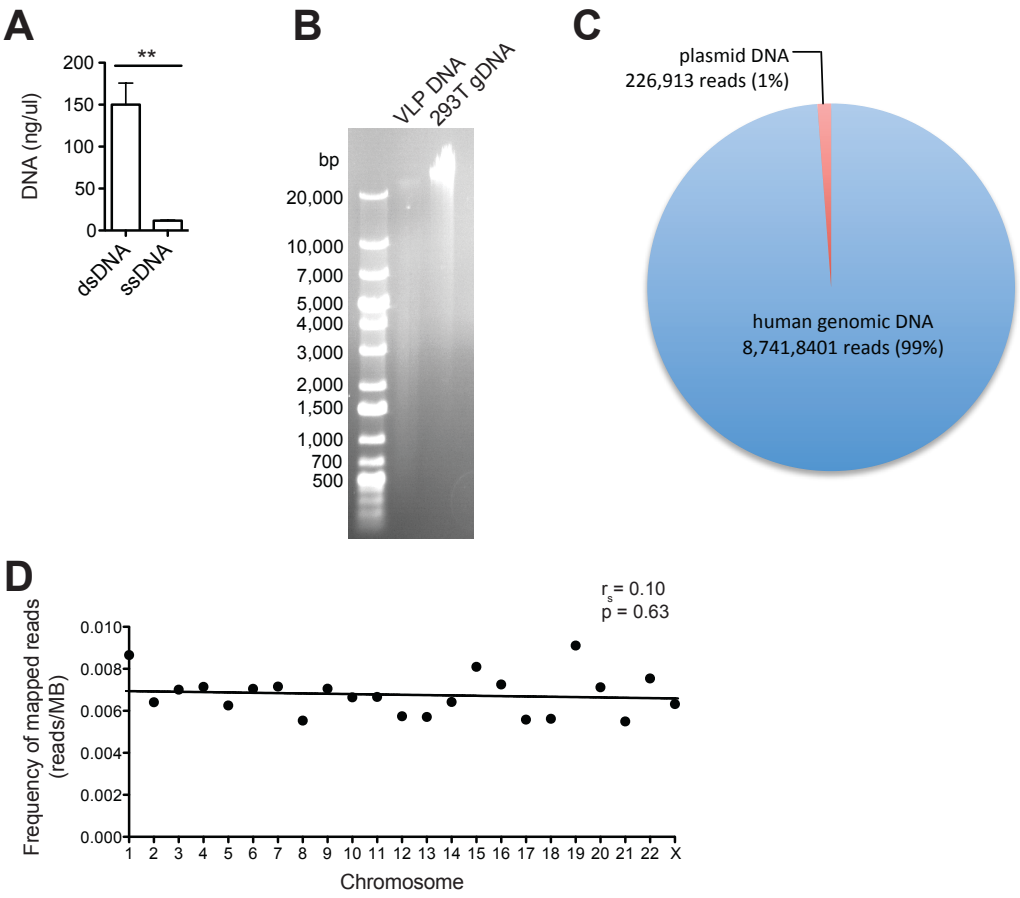

Fig. S8. Nonviral DNA in vector particle is primarily dsDNA, fragmented, and human genomic in origin. (**A**) Extracted DNA from LV preparation was analyzed for concentration of double-stranded and single-stranded DNA by fluoremtory-based assay. (**B**) Extracted DNA from LV prepation and from 293T cells was analzed by gel electrophoresis using EtBr staining. (**C, D**) Extracted DNA from LV prepations was deep sequenced and the reads mapped to the human genome (hg19) or plamid maps. Frequency and total mapped reads were quantified by origin (C). Frequency of reads and human chromosome number were subjected to Spearman's rank correlation analysis (D).

Table S1. Antibodies used in this study.

Antibody	Company	Clone/Cat No.
anti-human CD14	Biolegend	HCD14
anti-human CD86	Biolegend	IT2.2
anti-human DC-SIGN	Biolegend	9E9A8
anti-human HLA-DR	Biolegend	L243
anti-mouse B220	Biolegend	RA3-6B2
anti-mouse TCRB	Biolegend	H57-597
anti-mouse CD4	Biolegend	Gk1.5
anti-mouse CD8	Biolegend	53-6.7
anti-mouse CD11b	Biolegend	M1/70
anti-mouse CD11c	Biolegend	N418
anti-mouse CD44	Biolegend	IM7
anti-mouse CD62L	Biolegend	MEL-14
anti-mouse CD69	Biolegend	H1.2F3
anti-mouse CD74	BD Biosciences	ln-1
anti-mouse CD86	Biolegend	GL-1
anti-mouse F4/80	Biolegend	BM8
anti-mouse I-Ab	Biolegend	AF6-120.1
anti-mouse PDCA-1	Biolegend	129C1
anti-GFP	Santa Cruz Biotechnology	8334
anti-ovalbumin	Abcam	ab1221
anti-p24	Fitzgerald	10R-H120b
anti-phospho-p85 PI3K	Cell Signaling Technology	4228
anti-p85 PI3K	Cell Signaling Technology	19H8
anti-VSVG	Sigma-Aldrich	P5D4
EasySep™ Mouse Pan-DC Enrichment Kit	Stem Cell Technology	19763
SIINFEKL H-2Kb tetramer	NIH Tetramer Facility	

Table S2. Primer sets used in this study.

Target	*Forward sequence*	*Reverse Sequence*	*Notes*
VSV-G	TGAAGTGCCTTTTGTACTTAGCCTTTTTATTC	ACCAGCGGAAATCACAAGTAGTGACC	
amp^R	ACCAGCGGAAATCACAAGTAGTGACC	AAGCCATACCAAACGACGAGCG	
AluYd6 (human)	GAGATCGAGACCACGGTGAAA	TTTGAGACGGAGTCTCGTT	(*53*)
ACTB (human)	CATGTACGTTGCTATCCAGGC	ATTACCCACTCCCGACCCG	Primerbank ID 501885a1